CLoVER: an alterntive concept for damage interrogation in structural health monitoring systems

K. I. Salas   **C. E. S. Cesnik**
                         cesnik@umich.edu
Department of Aerospace Engineering,
The University of Michigan,
Ann Arbor, Michigan
USA

ABSTRACT

Structural Health Monitoring (SHM) is the component of damage prognosis systems responsible for interrogating a structure to detect, locate, and identify any damage present. Guided wave (GW) testing methods are attractive for this application due to the GW ability to travel over long distances with little attenuation and their sensitivity to different damage types. The Composite Long-range Variable-direction Emitting Radar (CLoVER) transducer is introduced as an alternative concept for efficient damage interrogation in GW SHM systems. This transducer has an overall ring geometry, but is composed of individual wedge-shaped anisotropic piezocomposite sectors that can be individually excited to interrogate the structure in a particular direction. The transducer is shown to produce actuation amplitudes larger than those of a similarly sized ring configuration for the same electric current input. The electrode pattern design used allows each sector to act as an independent actuator and sensor element, decreasing the number of separate transducers needed for inspection. The fabrication and characterisation procedures of these transducers are described, and their performance is shown to be similar to that of conventional piezocomposite transducers. Experimental studies of damage detection demonstrating the proposed interrogation approach are also presented for simulated structural defects.

NOMENCLATURE

b substrate half-thickness
c_j complex Fourier coefficients of shear tractions
c_g group velocity
C capacitance
d_{ij} piezoelectric coupling coefficient ($i, j = 1,2,3$)
D dispersion equation for Rayleigh-Lamb waves
$H_k^{(2)}$ hankel function of the second kind and order k
i $\sqrt{-1}$
I electric current
J_m bessel function of the first kind and order m
L rectangular actuator dimension
n number of half-cycles in toneburst signal
p capacitance function
r radial position
R radius
R_I transducer inner radius
R_O transducer outer radius
$s(t)$ toneburst signal
$S(\omega)$ fourier transform of toneburst signal
t time
$\bar{t}$ thickness
T substrate-actuator thickness ratio
$\bar{T}$ period
$u(.)$ unit step function
$\mathbf{u}$ displacement vector
V voltage
x, y cartesian co–ordinates
$\mathbf{\Gamma}$ coefficient matrix used in theoretical solution
$\delta(.)$ dirac delta function

Δr radial dimension
$\Delta \theta$ azimuthal dimension
ε_{ij} strain components ($i, j = x, y$ or r, θ)
θ_L transducer left azimuthal edge
θ_R transducer right azimuthal edge
μ, λ substrate material Lamé constants
ξ radial wavenumber
ρ substrate material density
τ_0 traction amplitude per unit length
σ stress tensor
ψ substrate-actuator stiffness-thickness ratio
ω angular frequency
ω_0 centre frequency of toneburst signal
a actuator
A antisymmetric mode
b bar (concentrated mass)
B substrate
h hole
p pulse
P piezoelectric
r reflection
s sensor
S symmetric mode
uc unit cell

1.0 INTRODUCTION

Structural health monitoring (SHM) is an integral part of damage prognosis systems. The primary function of this component is to inspect the condition of a structural element to detect damage and record its evolution in time. This task is typically accomplished using a network of actuators and sensors distributed around the structure. These transducers are connected to a central processing unit that processes and interprets the data received to detect and identify defects, if present. Guided-wave (GW) schemes have been considered for SHM applications due to the GW ability to travel over long distances with little attenuation, their active nature, and their sensitivity to different damage types.

There are multiple options for GW generation for SHM systems. A review of the state-of-the-art in this area was presented by Raghavan and Cesnik[1]. The most popular choices rely on piezoelectric materials as the active component of the device. Among these, the simplest option is surface-bonded piezoelectric wafers which have the advantages of being light, easy to handle, and inexpensive. However, their implementation in real structures is limited by their brittleness and lack of surface conformability. To overcome these difficulties, Bent and Hagood[2,3] developed the Active Fibre Composite (AFC) which used extruded cylindrical piezoceramic fibres encased between interdigitated electrodes and bonded using a structural epoxy. A similar concept, the Macro Fibre Composite (MFC), was later introduced by Wilkie et al[4], but in this case the piezoceramic fibers were diced using computer-controlled dicing saws resulting in a rectangular cross-section. These transducers (collectively referred to as Anisotropic Piezocomposite Transducers or APT), overcome the difficulties associated with piezoceramic wafers, and in addition have higher strain energy density due to the use of the 3-3 piezoelectric effect where the polarisation and primary strain direction are parallel. Another alternative that has been considered is interdigital Polyvinylidene fluoride (PVDF) transducers, where a homogenous piezoelectric substrate is excited through electrode fingers. Wilcox et al[5] developed this type of transducer in rectangular and wedge-shaped geometries, and showed that modal selectivity (defined as the selective excitation of specific GW modes) could be attained by controlling the width of the electrode fingers. However, the piezoelectric effect is weak in PVDF and it is therefore not well suited for sensing applications. Non-piezoelectric alternatives typically involve using electromagnetic acoustic transducer (EMAT) arrays. These devices involve a combination of concentric coils that work in conjunction with permanent magnets attached to the structure under inspection for GW excitation. These arrays have the advantage of being able to selectively excite specific wavelengths, but are rather bulky in comparison with piezoelectric alternatives. This approach has been pursued by Wilcox et al[6], who developed an omnidirectional transducer for damage detection using the fundamental symmetric (S_0) mode.

An important requirement for GW-based SHM systems is that power and complexity be minimised. A good transducer would focus all the input energy along a given direction on the structure to maximise the reflection levels from possible damage sites. In the case of monolithic wafers, due to their piezoelectric nature, the wave field induced is omnidirectional. Similarly, while APTs are able to generate directional wave fields, these transducers are unable to scan the entire structural surface individually. An option that has been explored in this regard is the use of phased arrays of piezoelectric wafers, where a group of transducers is employed to generate a scanning beam through signal interference. In this approach, each element in the array is excited with a modulated pulse and the response is recorded with all the remaining elements. This procedure is repeated until all independent combinations of actuator and sensor pairs have been used. The result from this scan is later used in a post processing algorithm that manipulates the phase of the pulses received to allow the array to virtually scan in a specific direction. Wilcox et al[7] used circular and linear arrays for the inspection of large areas of thick plate-like structures. Their study used both piezoelectric discs and shear piezoelectric transducers, and demonstrated that the ratio of the area covered to the array dimension was as large as 3000 to 1. Further efforts along this direction were presented by Fromme et al[8], who developed a ring array of piezoelectric transducers bonded on plate-like structures using a protective membrane. This concept was also successfully realised experimentally by Yu and Giurgiutiu[9,10], yielding very narrow GW scanning beams that were successful in identifying cracks. However, it was reported that the increased number of transducers needed produced wiring difficulties. More recently, Kim and Philen[11] extended this approach to consider arrays of APT devices. This interrogation architecture has also been extended to the case of composite laminated plates in the work of Zemmour and Pines[12]. The directionality achieved with phased arrays also has limitations, which are introduced by the presence of side lobes that inevitably result from the phased addition algorithm. These lobes are important because they determine the maximum signal to coherent noise ratio that the array can achieve, as explained by Wilcox et al[7]. If the array operates below this ratio, these side lobes may be misinterpreted as structural features or possible damage sites. Furthermore, while this type of array has been successful in obtaining directionality and detecting damage, the fact that this is achieved by the construction and destruction of waves implies that the power is not efficiently deployed. A different approach, based on MFC rosettes, was recently presented by Matt and Lanza di Scalea[13]. Their methodology was implemented using two rosettes in isotropic and composite plates as well as a curved honeycomb sandwich panel with satisfactory results. This method is not an active interrogation approach, but it is able to identify the direction of an incident wave which could for example have originated due to the interaction of a separate GW field with a damage site.

While GWs generated from traditional monolithic piezoceramic transducers cover all directions, this is achieved in an inefficient manner. On the other hand, transducer arrays achieve directional GW fields but at a high energy cost: directionality is based on construction/destruction of the signal during post-processing. Moreover, as discussed above, the system complexity associated with wiring decreases its reliability. In this paper, a novel transducer concept is presented that directs the GWs in an efficient way and keeps the electrical complexity to a minimum.
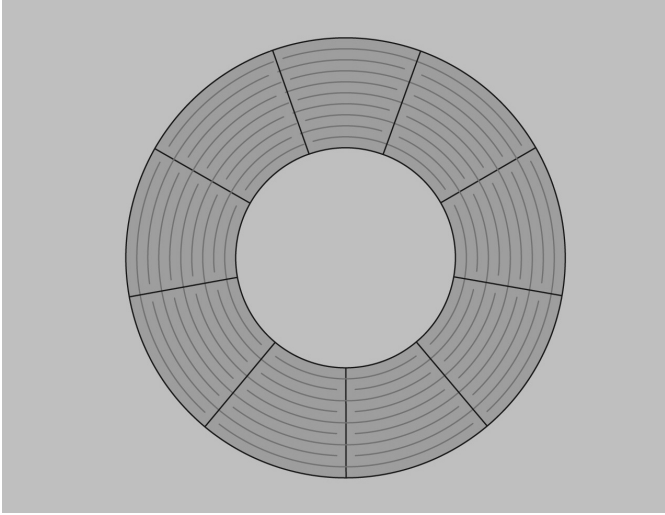
Figure 1. Schematic of the CLoVER transducer.

2.0 THE CLoVER TRANSDUCER

This paper presents a new transducer concept for efficient damage interrogation and GW excitation in SHM systems. The Composite Long-range Variable-direction Emitting Radar (CLoVER) transducer[14,15], schematically shown in Fig. 1, consists of a collection of wedge-shaped APT sectors arranged in a circular configuration. These transducers are able to efficiently scan a large structural area to identify the presence of defects from a central location, as schematically shown in Fig. 2. After exciting an individual sector with a modulated toneburst signal, a short time delay is introduced to record the reflected signals and allow all reflections from damage and structural features to attenuate. These reflections can be recorded using all sectors in the CLoVER transducer taking advantage of its sensing directionality, or by using a piezoelectric wafer sensor bonded, for instance, at the centre of the array. This procedure is then repeated until an entire 360° range has been covered. The experimental results presented in this paper demonstrate that each CLoVER sector uses the excitation input energy to primarily detect damage when it is located within its azimuthal projection.

An example of the transducer's ability to concentrate the actuation along a desired direction is illustrated in Fig. 2, which shows the out-of-plane displacements induced by a CLoVER sector with an azimuthal span of 30° for the fundamental antisymmetric (A_0) mode at 208kHz-mm. The figure shows the damage interrogation approach proposed with this new transducer, and it can be seen that the induced waves predominantly stay within the azimuthal bounds of each sector. Note that the results were obtained from the theoretical model reviewed in a subsequent section. It should be noted that, for illustration purposes, the GW field induced in the opposite direction (towards the centre of the transducer) has not been included in the figure.

A desirable feature for detecting damage using GWs is that the transducer be capable of selectively exciting individual modes. It is well known that different modes are necessary to identify a wide spectrum of damage types[16]. For instance, the S_0 Lamb mode is sensitive to through-the-thickness damage due to its dominant in plane component, and therefore is well suited to the detection of, for example, full- or part-depth holes. Similarly, the A_0 mode is better suited for surface damage (e.g., surface cracks) due to its dominant out-of-plane component. Furthermore, as higher-order modes are employed for damage characterisation, modal selectivity will play a more important role. The interdigitated electrode design used in the first generation of CLoVER transducers, described in section 3, uses two independent radial sub-divisions that can be used to obtain modal selectivity. This can be accomplished by selecting these dimensions according to the wavelength of the desired modes. An additional benefit of this feature is the ability of each CLoVER sector to act as an independent actuator and sensor unit in the array, as previously discussed. This would be advantageous in the field implementation of these devices as it decreases the number of separate transducers needed (both actuators and sensors) for data collection. Finally, due to their composite construction, CLoVER transducers have a higher specific strength than piezoceramic wafers, are more resistant to damage due to environmental conditions, and are easily bonded on curved surfaces characteristic of aerospace applications.

The following sections present a brief review of the theory of GW excitation by a CLoVER sector that serves as background to the parametric studies that illustrate some of the advantages of this transducer geometry over a ring configuration. The procedure used to manufacture these devices, as well as the characterisation studies conducted to verify its effectiveness, are subsequently described. Once the performance of the transducers has been established, experiments that illustrate the proposed interrogation approach are presented.
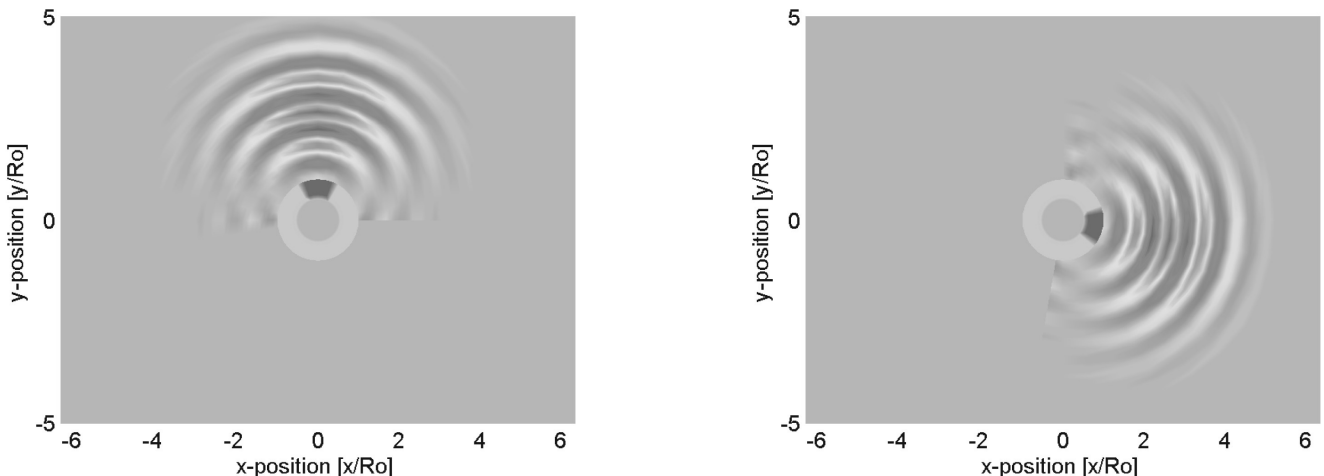

Figure 2. Damage interrogation approach used with CLoVER transducers: out-of-plane displacement field for A_0 mode at a frequency-thickness product of 208kHz-mm in an aluminum plate.

2.1 Review of GW excitation by a CLoVER sector

A theoretical model for the GW field excited by a CLoVER sector was presented in previous work by the authors[17,18]. The description of the problem considered an infinite isotropic substrate, and used the assumptions of perfect bonding and uncoupled substrate and actuator dynamics. As a result, their interaction was modeled through shear tractions along the transducer's radial edges on the substrate's surface. The problem was formulated using the 3D equations of elasticity for an isotropic material with the equilibrium equations expressed in displacement form as:

$$(\lambda + \mu)\nabla\nabla\mathbf{u} + \mu\nabla^2\mathbf{u} = \rho\ddot{\mathbf{u}} \qquad \qquad \text{...(1)}$$

where λ and μ correspond to the Lamé constants for an isotropic material and ρ represents the substrate material density. The equations were solved using Fourier transforms and complex variable techniques subjected to the following set of boundary conditions (for an infinite plate of thickness $2b$):

$$\boldsymbol{\sigma}(r,\theta,-b)\cdot\mathbf{n_l} = \mathbf{0} \qquad \qquad \text{...(2)}$$

$$\boldsymbol{\sigma}(r,\theta,b)\cdot\mathbf{n_u} = \boldsymbol{\sigma_0} \qquad \qquad \text{...(3)}$$

where $\mathbf{n}_l$ and $\mathbf{n}_u$ represent unit normal vectors to the lower and upper plate surfaces, respectively. The stress component σ_0 is given by:

$$\boldsymbol{\sigma}_0 = \begin{bmatrix} \sigma_{rz}^0 \\ 0 \\ 0 \end{bmatrix} \qquad \qquad \text{...(4)}$$

and the only non-zero stress component is expressed as:

$$\sigma_{rz}^0 = \tau_0\big(u(\theta-\theta_L) - u(\theta-\theta_R)\big)\big(\delta(r-R_I) - \delta(r-R_O)\big) \qquad \text{...(5)}$$

where the term τ_0 corresponds to the traction amplitude per unit length that the transducer exerts on the substrate, $u(.)$ represents the
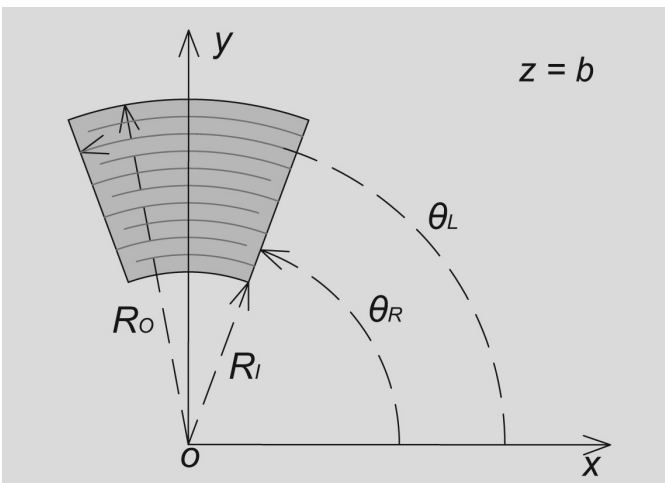

Figure 3. Geometry of a CLoVER sector.

unit step function, and $\delta(.)$ represents the Dirac delta function. Note that the form of Equation (5) makes the stresses non-zero only along the radial edges of the transducer. These are represented through the outer and inner radii (R_O and R_I respectively), and the transducer's right and left azimuthal edges (θ_R and θ_L respectively), as shown in Fig. 3.

The time-dependent Cartesian displacement components for the A_0 mode, expressed in polar coordinates r and θ, result in[17,18]:

$$\mathbf{u}_A(r,\theta,t) = \frac{1}{2\pi}\int_{-\infty}^{\infty}\sum_{\xi_A}\left(\sum_{k=-\infty}^{\infty}\frac{i\pi^2\Gamma_A}{\zeta_k(\theta)D_A^{'}}\Delta_A H_k^{(2)}(\xi_A r)\right)S(\omega,\omega_0)e^{i\omega t}\mathrm{d}\omega$$

$$\text{...(6)}$$

where ξ_A represents the propagating wavenumber for the antisymmetric mode, Γ_A is a matrix of coefficients, Δ_A is a vector containing the source terms, and $D_A^{'}$ represents the derivative of the Rayleigh-Lamb dispersion equation for antisymmetric modes with respect to the wavenumber, ξ. A detailed definition of these parameters may be found in a separate work by the authors[18]. In addition, the term ζ_k is defined as:

$$\zeta_k \equiv e^{i\frac{\pi}{2}k}e^{ik\theta} \qquad \qquad \text{...(7)}$$

The outward propagating radiation pattern is introduced by the Hankel function of the second kind, $H_k^{(2)}(\xi_A r)$. The term $S(\omega, \omega_0)$ corresponds to the Fourier transform of the time-dependent part of the excitation which, for SHM applications, is typically given by a Hann-modulated toneburst at a centre frequency ω_0.

2.2 Parametric studies on transducer dimension

In this section, the effect of the radial and azimuthal dimension of a CLoVER sector on the induced displacements is explored. This is done by examining the variation of the source term corresponding to the out-of-plane displacements, $\Delta_A^{(3,1)}$. This choice is justified by the observation that the induced displacements have separate contributions from the transducer geometry and the wave propagation parameters of the substrate (referred to as the excitability function). The source term per unit length along the thickness direction corresponding to the out-of-plane component can be expressed as:

$$\Delta_A^{(3,1)} = \alpha_{1-k}^{(1)} + \alpha_{-1-k}^{(2)} \qquad \qquad \text{...(8)}$$

where k represents a summation index and the terms α, for a given index j, are defined as:

$$\alpha_j^{(1)} = \frac{1}{2}\big(c_j^{(1)} + ic_j^{(2)}\big)(-i)^j X_j \qquad \qquad \text{...(9)}$$

$$\alpha_j^{(2)} = \frac{1}{2}\big(c_j^{(1)} - ic_j^{(2)}\big)(-i)^j X_j \qquad \qquad \text{...(10)}$$

with each component having the following definitions[17, 18]:

$$\begin{bmatrix} c_j^{(1)} \\ c_j^{(2)} \end{bmatrix} = \frac{1}{2\pi}\int_0^{2\pi}\big(u(\theta-\theta_L) - u(\theta-\theta_R)\big)\begin{bmatrix} \cos\theta \\ -\sin\theta \end{bmatrix}e^{ij\theta}\mathrm{d}\theta \qquad \text{...(11)}$$
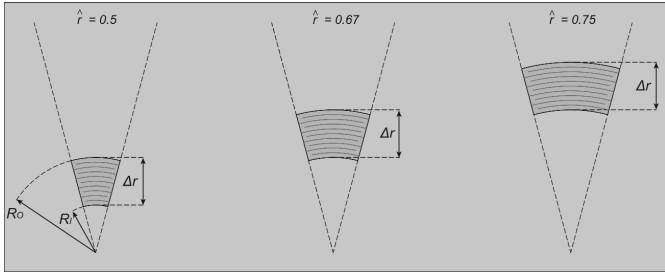
Figure 4. Schematic illustrating that different combinations of inner and outer radii can yield similar radial dimensions in a CLoVER sector.

Figure 5. Effect of radial dimension on CLoVER sector frequency response for $\Delta r / b$ = 75 and $\Delta\theta$ = 15°.

$$X_j = 2\pi \left(\frac{R_O}{b} J_j \left(\xi * \frac{R_O}{b} \right) - \frac{R_I}{b} J_j \left(\xi * \frac{R_I}{b} \right) \right) \qquad ...(12)$$

The form of the Equations (9) through (12) results from the definition of the Fourier transform of the stress exerted on the substrate by the transducer, Equations (5)[17,18]. Observe that the non-dimensional form of the wavenumber used, $\xi* = \xi b$, generalises the expression to any substrate thickness. Also note that the source term is given by a sum over the index k which also has contributions from the radiation pattern. Since the expression to be analysed is the result of this sum, the two components cannot be separated. Hence, the term considered in the parametric studies is of the form:

$$\sum_{k=-\infty}^{\infty} \frac{1}{\zeta_k} \Delta_A^{(3,1)}(k, \xi, R_I, R_O, \theta_L, \theta_R) H_k^{(2)}(\xi r) \qquad ...(13)$$

For all parametric studies, the azimuthal position is fixed along the transducer centreline so that the function ζ_k is equal to one. Similarly, the radial position selected remains fixed at $r = 15R_O$. The effect of the transducer radial dimension is studied first. Due to the geometry of a CLoVER sector, there are two important parameters related to its radial dimension. The first of these is the radial length itself. However, as shown in Fig. 4, this parameter is not sufficient to fully characterise the geometry of the transducer as different combinations of inner and outer radii can yield a similar result. It is intuitively expected that this difference in the geometry would manifest itself in the frequency response of the transducer. Consequently, the parameter $r*$ defined in the manner described below is used:

$$r* = \frac{R_I}{R_O} \qquad ...(14)$$

In the parametric studies conducted a value of $r*$ is specified, and the position of the transducer radial edges is changed so as to maintain a constant dimension. For each of these, the sum given by Equation (13) is computed over a range of frequencies from 1kHz to 800kHz in increments of 0·5kHz. In order to isolate the effect of the transducer dimension, the results are plotted as a function of the radial length, Δr, normalised by the wavelength, λ, which is a function of the frequency. Note that this approach yields results that are valid for both the S_0 and A_0 modes. However, it is important to emphasise that the transducer dimension itself will be different for each mode due to their different wavelengths. The result of this analysis is shown in Fig. 5, where a fixed azimuthal span of 15°, a fixed radial dimension $\Delta r = 75b$, and various values of $r*$ were used. There are several important features in this result. First, note that the amplitude of the response decreases as the transducer radial dimension is increased. This effect is partly due to the attenuation induced by the term $H_k^{(2)}(\xi r)$. As the frequency is increased, the
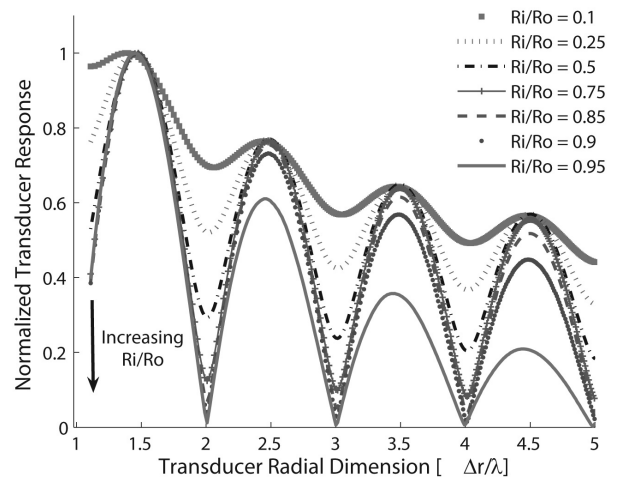
increasing wavenumber results in a larger number of wavelengths between the transducer outer radius and the measurement point (which remains constant). Since the amplitude of the propagating wave decays with the number of wavelengths, smaller amplitudes are observed as the ratio $\Delta r / \lambda$ increases. Furthermore, for the azimuthal dimension considered, the decay in amplitude is only dependent on the attenuation as all the local minima (with the exception of $r* = 0·95$) are coincident. A more important observation, however, is that for low values of the ratio $r*$ the response amplitude does not display any zeros. Instead, a series of local extrema is observed where the minima occur when the radial dimension coincides with integer multiples of the wavelength and the maxima correspond to points where this dimension is a factor between 0·35 and 0·5 integer multiples of the wavelength. As the ratio is increased, the local minima progressively approach zero while the local maxima remain essentially unchanged. Note that the location of these points is similar to the case of a rectangular transducer. Since for low values of $r*$ the transducer response does not display any zeros, modal selectivity cannot be attained. This feature is typically obtained by selecting the transducer dimension so as to operate at a frequency node for a specific mode. When testing below the threshold of the higher Lamb modes (where only the S_0 and A_0 mode exist), this results in the displacement components being composed of only the opposite mode. This observation provides important insight into the nature of modal selectivity attained with finite dimensional transducers. As the value of $r*$ increases, the geometry of the CLoVER sector approaches that of a rectangle. This geometric configuration is in turn symmetric with respect to an axis normal to the fibre direction. This indicates that modal selectivity is directly related to the symmetry of the transducer relative to the wave propagation direction. For low values of $r*$, the CLoVER transducer sector asymmetry with respect to such an axis is very strong and modal selectivity cannot be obtained. Therefore, for applications where modal selectivity is needed, larger values of $r*$ should be selected. The specific value will depend on the level of modal selectivity needed. For example, if one of the modes needs to be largely attenuated, then $r*$ should be in the order of 0·9. Conversely, for applications where a transducer with high gain over a large frequency range is desired, low values of $r*$ should be used.

The effect of the azimuthal dimension is shown in Figs. 6 and 7 for a similar range of values of $r*$. Note that as the span is increased the location of the local extrema remains essentially unchanged. It can also be observed that the amplitudes of the local minima decrease significantly, especially for larger values of $r*$. In addition, the amplitude of the local maxima does not decay in the same
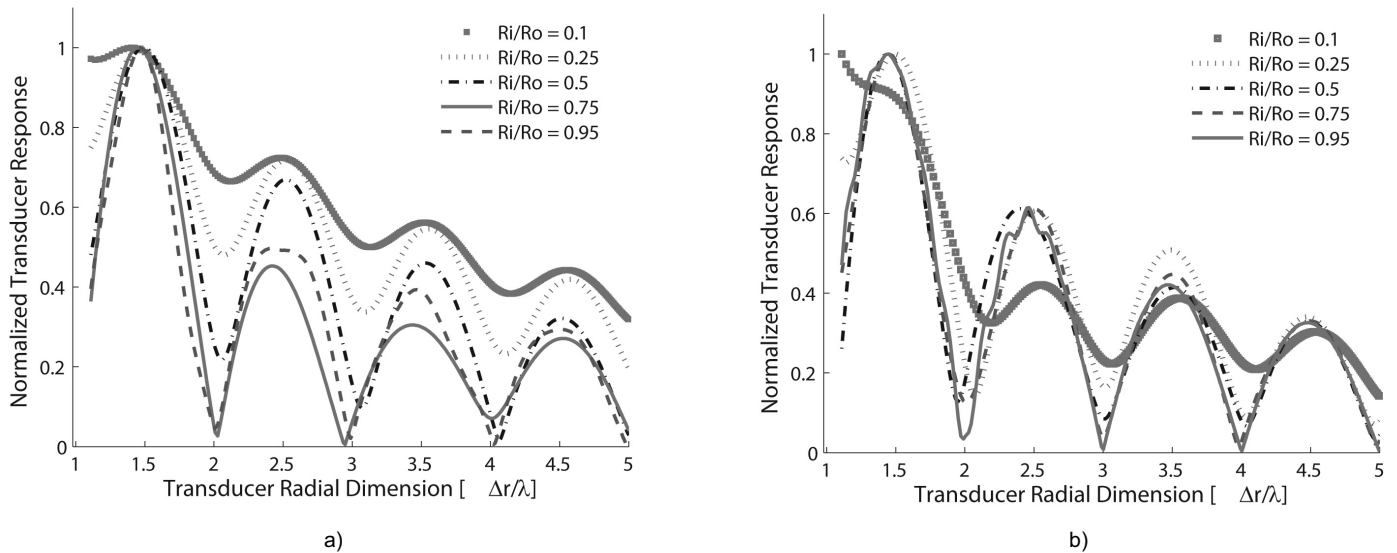
Figure 6. Effect of radial dimension on CLoVER sector frequency response for
$\Delta r/b$ = 75 and (a) $\Delta\theta$ = 45°; (b) $\Delta\theta$ = 90°.
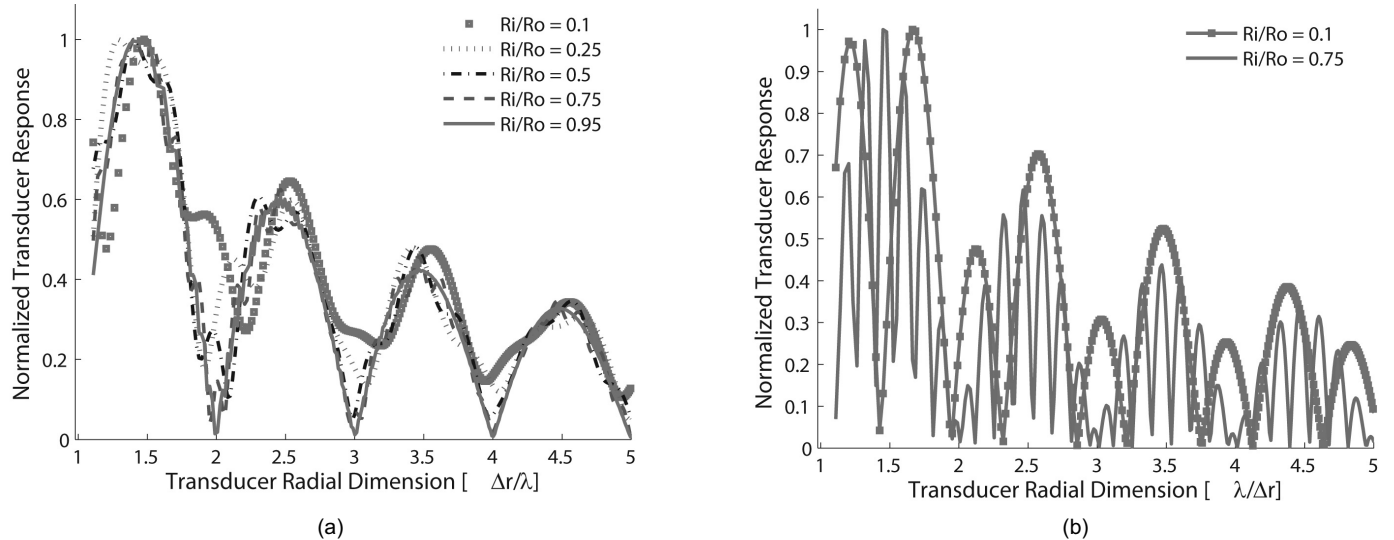

Figure 7. Effect of radial dimension on CLoVER sector frequency response for $\Delta r/b$ = 75 and (a) $\Delta\theta$ = 2,700; (b) ring configuration.

manner for larger azimuthal spans. This effect, however, does not appear to follow a consistent pattern and the identification of its source is further complicated by the presence of the attenuation term in Equation (13). Nevertheless, as the location of the local extrema is not significantly altered, this effect is not critical. From these results, it can be concluded that the azimuthal span of the transducer has a secondary effect on the frequency response for the range of values of interest for use in CLoVER transducers ($\Delta\theta$ < 90°). This parameter may therefore be selected based on a different criterion as, for example, the directionality desired.

A potential evolution of the CLoVER transducer that takes advantage of the directionality of the induced GW field and the ability to interrogate a complete 360° range is shown in Fig. 8. This device would be composed of a piezoceramic ring with the fibres diced in a manner such that the active sectors have a rectangular shape. This device would incorporate the modal selectivity attainable with this transducer geometry which is often critical in SHM applications.

2.3 Performance improvement offered by CLoVER sector geometry

As explained in the theory review section, the displacement field is proportional to the traction amplitude per unit length, τ_0, exerted along the radial edges of the APT. This leads to the intuitive conclusion that actuators with longer edges exert a larger 'net traction'. In the case of a wedge-shaped geometry, the limiting case is a ring configuration where the length of the radial edge is maximised for fixed inner and outer radii. In this section, we seek to relate the traction per unit length to an electric input metric to explore the increase in performance that can be obtained by the CLoVER sector geometry. To do this, the piezoelectric strain induced by the APT must be considered. Several approaches have been proposed to model the interaction between a structural substrate with a surface bonded piezoelectric actuator under static conditions. This type of analysis generally employs an assumed strain field for the substrate, while the actuator is typically modeled as having a
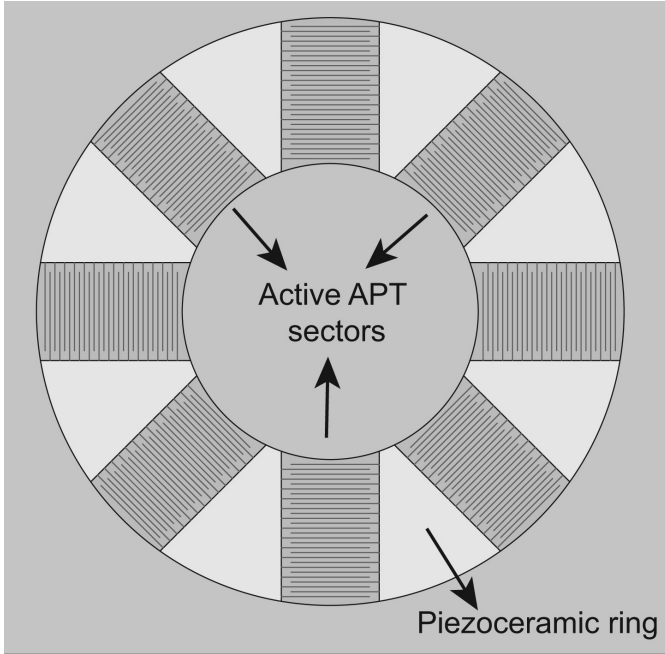
Figure 8. Potential evolution of the CLoVER transducer.

constant through-the-thickness strain. Crawley and de Luis[19] considered this type of problem using a linear strain distribution for the substrate, which was modeled as an Euler-Bernoulli beam. Their analysis, however, consisted of two surface bonded piezoelectric actuators which resulted in a symmetric system. Chaudry and Rogers[20] conducted a similar study using a linear strain distribution for the actuator and substrate under the assumption of perfect bonding. They provided an expression for the curvature induced on the substrate by a single surface-bonded actuator, from which the force per unit length could be determined using the substrate's cross-sectional properties. In order to obtain a functional relationship between the traction per unit length and the input voltage, this result will be employed here. It must be emphasised that this is an approximation as the mechanics of the substrate in this work are not those of Euler-Bernoulli beams. Then, for a rectangular cross-section, the force per unit length induced along the edges of the actuator can be expressed as:

$$\tau_0 = \frac{4E_B b T(1+T)\psi}{6T + 4T^2 + 4 + \psi T^2 + 1}\varepsilon_P \qquad ...(15)$$

where T is defined by:

$$T = \frac{2b}{\overline{t_a}} \qquad ...(16)$$

and ψ represents the stiffness-thickness ratio given by:

$$\psi = \frac{2E_B b}{E_a \overline{t_a}} \qquad ...(17)$$

Finally, the piezoelectric strain can be expressed through:

$$\varepsilon_P = d_{33}\frac{V}{d_{IDE}} \qquad ...(18)$$

where d_{IDE} represents the centre-to-centre distance between any two fingers in the APT interdigitated electrode. Note that Equation (18) implies that a uniform electric field through the radial length of the actuator is assumed. In actual APT devices this is not the case since the electric field lines originate and end at the interdigitated electrode fingers. Since the field lines must be normal to the surfaces where they originate and end, there exists a small region close to the electrode fingers where the lines are not oriented along the fibre direction. Nevertheless, it has been shown that this is a reasonable simplification if the distance between any two electrode fingers, d_{IDE}, is sufficiently large. For instance, the work of Nguyen and Kornmann[21] concluded that a minimum electrode spacing of 1·1mm would be required to obtain a homogenous electric field along the length of the fibre for AFCs. If the APT is modeled as a capacitor with capacitance C, then a suitable metric for the electric input is the electric current drawn, I. For a harmonic input voltage of amplitude V at a frequency ω, the magnitude of the electric current is given by:

$$I = \omega C V \qquad ...(19)$$

At this point, it is necessary to determine the dependence of the APT capacitance on the transducer's radial and azimuthal dimensions. The capacitance of this type of transducer is typically analysed using the repetitive nature of the interdigitated electrode pattern. In this way, only the electric field in a representative unit cell, defined as the region between any two electrode fingers, is considered. A comprehensive study on this electric field was conducted by Lloyd[22] using conformal mapping techniques. In that work, it was shown that the capacitance of each unit cell was primarily determined by the piezoceramic thickness, electrode finger width, and electrode finger spacing, while it scaled linearly with electrode finger length. Thus, the capacitance of a unit cell can be expressed as:

$$C_{uc} = p(k,\varepsilon_0, d_{IDE}, \overline{t_a})L_{IDE} \qquad ...(20)$$

where, in the case of a CLoVER sector, the electrode finger length is determined by its radial position, r_{IDE}, and the transducer's azimuthal span, $\Delta\theta$, so that:

$$C_{uc} = p(k,\varepsilon_0, d_{IDE}, \overline{t_a})r_{IDE}\Delta\theta \qquad ...(21)$$

A closed form expression for the function p cannot be readily obtained. However, the work of Lloyd[22] showed that this function is non-linearly dependent on the electrode finger and unit cell geometry, and that it increases exponentially as the centre-to-centre distance between the electrode fingers approaches zero. It is also important to note that any contribution from the capacitance of the epoxy has been neglected. This is a logical choice since its dielectric constant ($k \sim 6$)[23] is much smaller than that for a typical piezoelectric ceramic ($k \sim 1,700$, PZT-5A)[24]. The capacitance of the overall device may be obtained by considering it as a composition of capacitors connected in parallel. Then, the capacitance of each unit cell may be simply added together which results in:

$$C_{uc} = p(k,\varepsilon_0, d_{IDE}, \overline{t_a})\left(\frac{R_O + R_I}{2}\right)\Delta r\Delta\theta \qquad ...(22)$$

The results given by Equations (15), (18) and (22) combined with the definition of Equation (19) indicate that the current drawn by the actuator will be linearly proportional to the product of the traction per unit length, τ_0, and the APT capacitance. This result further

indicates that the actuator with largest angular span will draw the largest current in order to maintain a constant τ_0. Even though the ring-configuration draws the largest current according to the conclusion above, there are several shortcomings with its performance. For example, the GW field excited has the same amplitude in every direction and therefore no focusing is possible. A CLoVER sector offers an improvement over these shortcomings, especially if the same current input as in the case of the ring is utilised. Due to its geometry, this configuration is able to concentrate a significant portion of the excitation along the intended scan direction. Similarly, due to its shorter azimuthal span, the larger current input yields a larger magnitude for τ_0, and hence an increased displacement amplitude everywhere. This effect can be quantified using the relationships provided by Equations (19) and (22). Equating the currents drawn by the ring-shaped APT and a CLoVER sector yields:

$$\omega p \Delta \theta \frac{R_O + R_I}{2} \Delta r V^{CLoVER} = \omega p 2\pi \frac{R_O + R_I}{2} \Delta r V^{Ring} \qquad ...(23)$$

from which, according to Equations (15) and (18), it follows that:

$$\frac{\tau_0^{CLoVER}}{\tau_0^{Ring}} = \frac{2\pi}{\Delta \theta} \qquad ...(24)$$

A sample result from this analysis is presented in Figs. 9. The figures illustrate the peak-to-peak amplitude of the out-of-plane displacement component for the S_0 (Fig. 9(a)) and A_0 (Fig. 9(b)) modes at a frequency-thickness product of 150kHz-mm and 500kHz-mm respectively. The result is represented through polar plots where the radial distance from the origin corresponds to the peak-to-peak amplitude at each azimuthal position. The transducer centreline is oriented along the 90^0 direction in the figure. The results for each azimuthal span considered were normalised by those

corresponding to a ring geometry to illustrate the performance gain offered by the CLoVER geometry. For the particular combination of parameters shown, the out-of-plane displacement for a CLoVER sector with an azimuthal span of $15°$ can be made more than six times larger than that corresponding to a ring for the S_0 mode, while in the case of the A_0 mode they are increased by a factor of approximately eight. The results presented in Fig. 9 must be carefully interpreted, however, as they do not imply that using a CLoVER transducer will result in the displacement amplitudes being automatically increased. Instead, the implication is that as the array is divided into individual sectors, the electric current needed to obtain a given displacement amplitude using a ring geometry can be more efficiently used. In addition to their increased amplitude, the induced displacements will also be focused along a desired direction as shown by the directionality of the main lobe. The result given by Equation (24) may also be used to quantify the improvement obtained by reducing the CLoVER azimuthal span from a given reference value.

3.0 TRANSDUCER FABRICATION

A sample interdigitated electrode pattern design used in the first set of CLoVER transducers is shown in Fig. 10. The original layout was designed using a CAD application and then transferred onto a copper-clad kapton film (Pyralux LF7062R) using photolithography (MetroCircuits[†]). This material has a layer of rolled-annealed copper on the kapton film, which has a thickness of 25μm, with an adhesive thickness of 13μm, and a copper density of 153g/m². Each electrode finger has a width of 0·1mm, while the separation distance between any two was set at 0·5mm. These values are similar to those used in NASA-standard MFCs[25,26]. As previously mentioned, the overall design consists of two independent radial subdivisions that allow the length of the active fibres in a given sector to be electrically varied. PZT-5A was selected as the active piezoceramic material in these
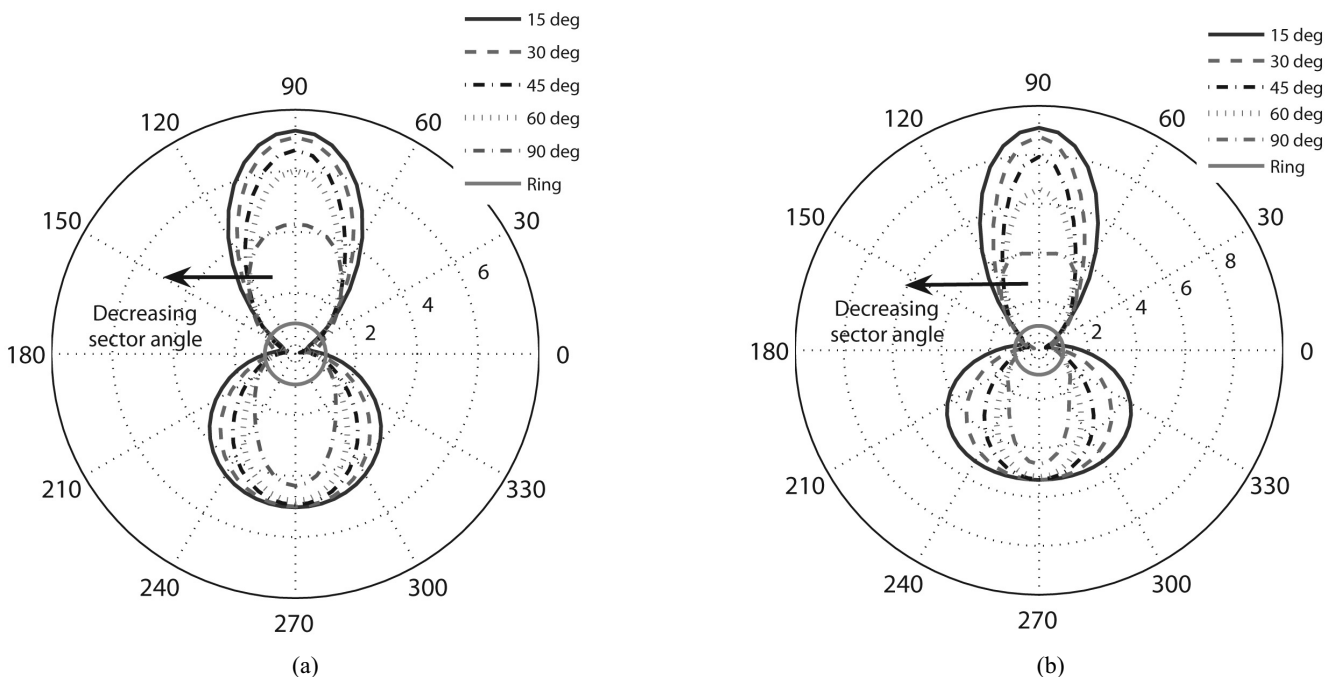

Figure 9. Improvement in peak-to-peak amplitude of out-of-plane displacement offered by the CLoVER geometry over a ring configuration for (a) S_0 mode at 500kHz-mm, and (b) A_0 mode at 150kHz-mm in an aluminum plate.
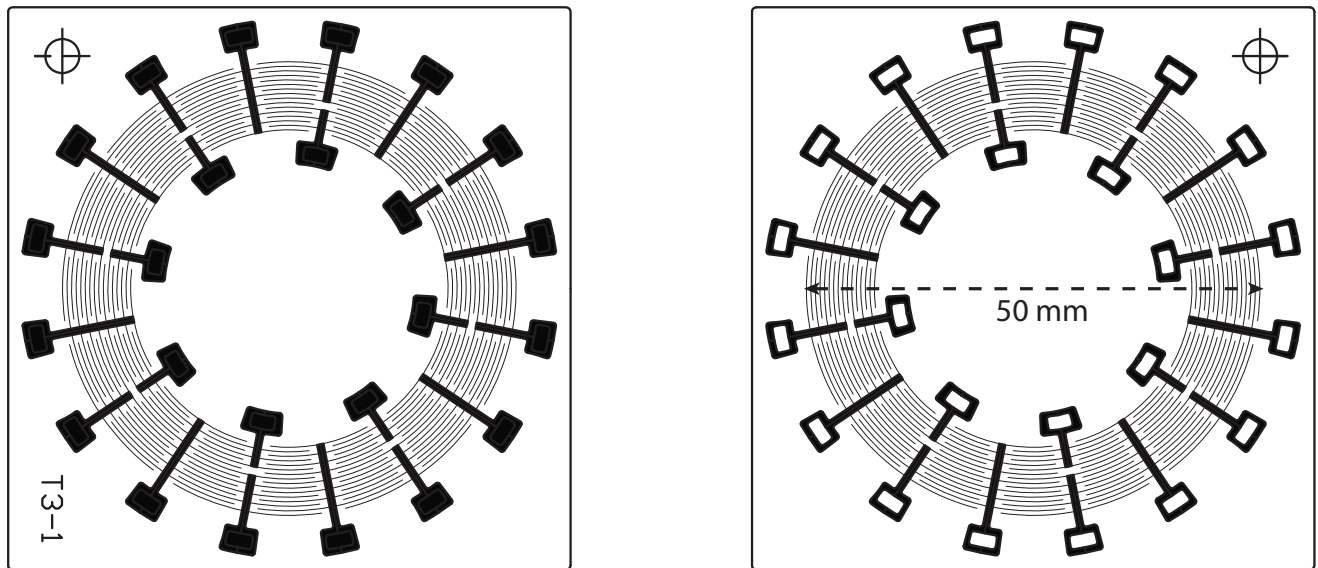
Figure 10. Sample interdigitated electrode pattern used in CLoVER transducers.

transducers. This material was obtained in ring shaped units with a thickness of 0·2mm (EBL Products[†]), and these wafers were subsequently diced into fibres using a computer controlled dicing saw (American Dicing[‡]). The dicing angle was selected so that the fibre width at the inner radius position was equal to the prismatic fibre width used in conventional MFC transducers (0·36mm). These fibres remain in position by being attached to a blue carrier film.

The electrode patterns and the piezoceramic fibres were assembled together using an epoxy adhesive system (Hysol Loctite E-120HP). As the blue carrier film where the fibres are attached must be removed, two cures are necessary. The first cure, referred to as partial cure, is needed to remove the film while keeping the relative orientation of the fibres. The final cure is needed to completely cure the epoxy and finalise the device. This sequence of steps is similar to the one presented by Wilkie and High[4]. However, in that work, the transducers were cured in a vacuum hot press, and therefore some details of the procedure were modified in this work to adjust it to an autoclave cure. All assembly procedures were done similar to those presented in the standard manufacturing procedure[4]. For the autoclave cure, the curing parameters presented by Wilkie and High[4] were used as a starting point. These indicate that the transducers must be partially cured at a temperature of 46°C (115°F) for five minutes at a pressure of 483kPa (70psi), while the final cure must be performed at 121°C (250°F) for a minimum of two hours at a similar pressure. These temperatures have been shown to yield satisfactory cure levels using cure kinetics models[27]. Prior to both cures, a vacuum dwell (–28 in Hg) of at least 15 minutes is necessary. Moreover, this vacuum must be maintained throughout the cure cycles.

During initial tests, it was found that the recommended 483kPa curing pressure did not yield a satisfactory compaction level in the final transducer. As a result, the pressure was increased to 690kPa (100psi) during both partial and final cures. During the final procedure, the pressure during partial cure was reduced to 552kPa (80psi) as it was found that, due to the increased pressure, pieces of the blue carrier film were permanently attached to the piezoceramic fibres. In order to facilitate the removal of air bubbles, an additional dwelling time of 15 minutes was added during the final cure after reaching the maximum pressure but prior to the increasing the

temperature. There was no modification to the temperatures during partial and final cure. The actual cure cycles used (both temperature and pressure) are shown in Fig. 11.

The final step in the manufacture process is the poling of the device. During this step, the piezoelectric domains in the piezoceramic material are aligned resulting in a net polarisation. In the case of APTs, the polarisation direction coincides with the fibre direction. The standard procedure specifies that the device must be poled at an electric field of 3kV/mm (1·5kV with an interdigitated electrode spacing of 0·5mm assuming a uniform electric field[†]) for five minutes at room temperature. However, during initial tests it was found that the high voltage resulting from this electric field requirement sometimes resulted in failure of the transducer during poling, and did not yield satisfactory strain performance. In general, the net polarisation in a piezoelectric device is dependent on the poling field, poling time, and poling temperature. The primary requirement to achieve a net polarisation is that the poling field be larger than the coercive field for the specific device (in principle, the longer the poling time the larger the net polarisation will be). Preliminary experimental tests indicated that for the transducers developed in this work, this field was in the order of 2kV/mm at room temperature. This value is expected to decrease with increasing temperature until approximately 90°C as indicated by Bent[3]. Therefore, in order to increase the strain performance of the transducers while reducing the possibility of failure, the poling time and temperature were increased, while the poling voltage was decreased. Prior to deciding the poling time, several sample MFCs were constructed following the procedure specified above, and poled for different times. These were later characterised following the procedure presented in the Transducer Characterisation section to determine how the increasing time altered the strain performance of the devices. These results, summarised in Table 1, show that increasing the poling time produces a significant improvement in the performance of the transducers.

As mentioned earlier, increasing the poling temperature decreases the coercive field, which would allow the transducers to be poled for a shorter time and lower field while still maintaining acceptable

---

[†] The poling parameters will be expressed in electric field form from this point on. This convention assumes a uniform electric field distribution between any two interdigitated electrode fingers, which corresponds to the maximum possible magnitude of the field along the poling direction.
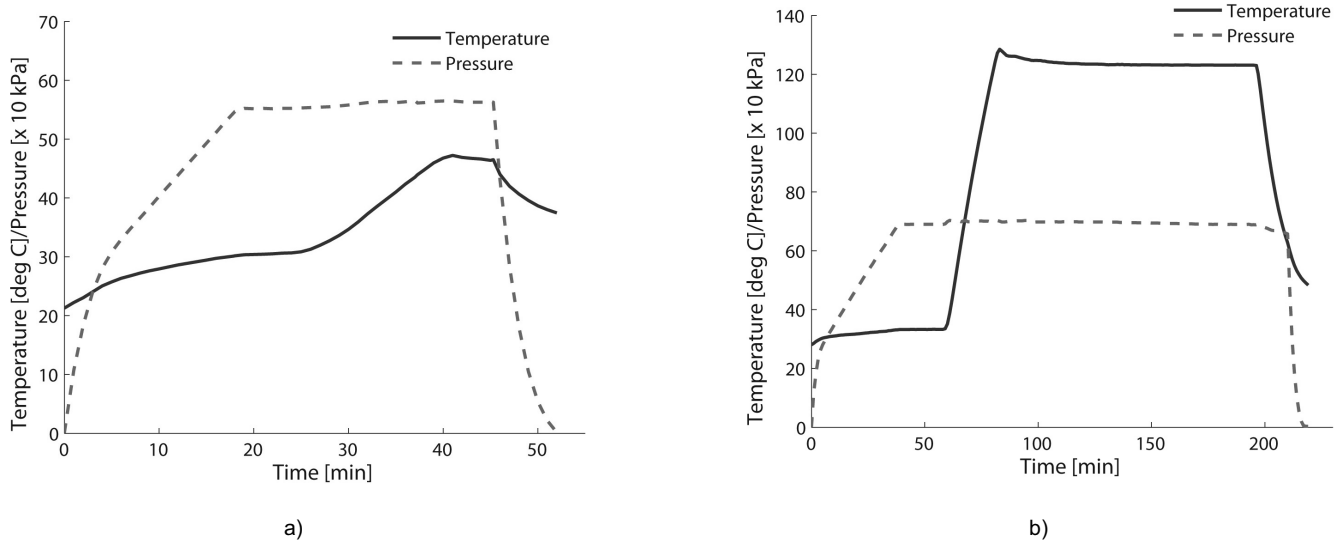
Figure 11. (a) CLoVER partial cure cycle; (b) CLoVER final cure cycle.

Table 1
Summary of transducer performance under different poling times

Transducer Index	Poling Field [kV/mm]	Poling Time [min]	$V_{p\text{-}p}$ [V]	$\mu\varepsilon_{p\text{-}p}$	d_{33} [$\times 10^{-10}$ m/V]
1	2·22	15	252·4 + 1·1	52·6 + 1·5	1·04 + 0·03
2	2·22	30	251·9 + 0·2	60·3 + 0·9	1·20 + 0·02
3	2·22	60	252·0 + 0·4	111·9 + 1·6	2·22 + 0·03

performance. As a result, the transducers were poled at an electric field of 2·4kV/mm for 30 minutes at an average temperature of 87°C using an industrial oven. During this procedure, the voltage was increased in steps of 20V, with a holding time of 5 seconds between steps. The holding time was increased to 20 seconds when a 100V increment was reached. An Agilent 33220A arbitrary waveform generator was used in conjunction with a Trek PZD 2200 high voltage amplifier (with a fixed gain of 200) to supply the necessary voltage.

4.0 TRANSDUCER CHARACTERISATION

The objective of the characterisation studies is to verify the quality of the curing and poling procedures described in section 3. Strain gauges were bonded on several transducers along the fibre direction to measure the axial strain. The CLoVER transducers were instrumented with EA-06-125AD-120 strain gauges from Measurements Group, which covered approximately nine electrode fingers. In this case, the centreline of the strain gage was aligned with the centreline of the transducer. As the unidirectional strain gage is insensitive to transverse strains, there is some unavoidable error in the readings due to the curved geometry of the fibre disposition. Consequently, the strain recorded for the CLoVER transducers is expected to be an underestimate of the actual value. The in-house rectangular transducers were instrumented with EA-06-250AD-350, which covered approximately 18 electrode fingers. The gages were bonded using M Bond AE-150 bonding agent from Measurements Group which was cured for two hours in an oven at 65°C according to the manufacturer's instructions. The transducers obtained from NASA were instrumented with CEA-13-250WQ-350 strain gages which are able to simultaneously measure strains along two perpendicular

directions[28]. The voltage input was provided using the same waveform generator described in the Transducer Fabrication section and a Krohn-Hite Model 7500 wide band amplifier. Various voltage inputs were used throughout the tests, while the frequency was maintained constant at 0·1Hz to simulate quasi-static conditions. Furthermore, during testing, the transducers were left to hang under their own weight to obtain their free response. The strain gage signal was conditioned and amplified using a Vishay 2311 signal conditioning amplifier and recorded using a digital oscilloscope. The experimental setup is shown in Fig. 12(a) while the strain gage-CLoVER arrangement can be seen in Fig. 12(b).

The results from these studies are shown in Fig. 13. Clearly, the manufacturing and poling procedures implemented in section 3 yield actuators with performance levels comparable to those obtained using the standard NASA manufacturing procedure. As it was previously mentioned, it is likely that the lower results seen for the CLoVER transducer are due to the unavoidable misalignment between the electrode and gage patterns. Nevertheless, for the peak-to-peak voltage of interest in SHM applications (up to ~400V), these differences are acceptable. Having determined the performance of the CLoVER transducers, the next section discusses their implementation in preliminary damage detection experiments.

5.0 DAMAGE INTERROGATION USING CLoVER TRANSDUCERS

The objectives of the experimental tests presented in this section are to evaluate the interaction of the GW field induced by a CLoVER sector with simulated damage, and to demonstrate the damage interrogation approach proposed with this new transducer. Two different simulated damage types were considered, namely, a concentrated mass and a
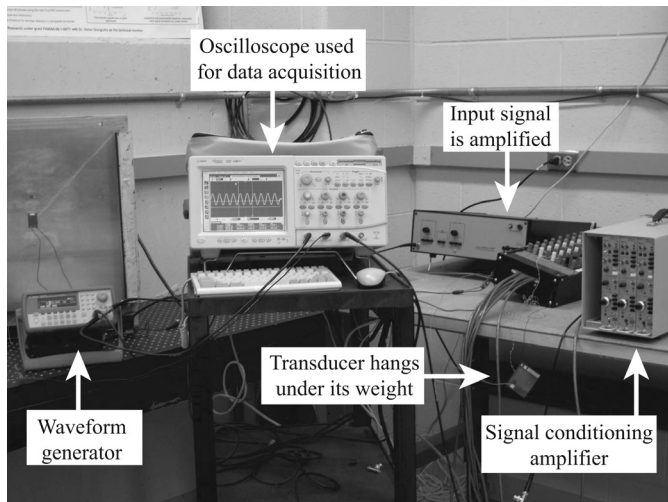
(a)
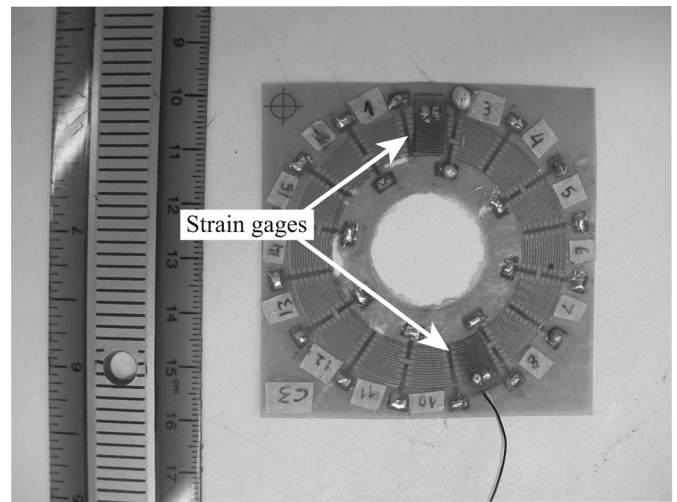
(b)

Figure 12. (a) Experimental setup for transducer characterisation; (b) Detail of CLoVER transducer instrumented with strain gages.

through-thickness hole. This section describes the overall experimental setup while the specific details and results for each damage type are presented in the subsequent sections. A square aluminum 5005 plate with a side length of 0·7m and a thickness of 3·2mm was used in the experimental tests. The plate was supported by unistrut bars on two sides and was free on the remaining two sides. A CLoVER transducer was bonded on the surface of the plate at its geometric centre by applying a thin layer of Epotek 301 bonding agent and allowing it to cure for 24 hours. The active CLoVER sector used had a radial dimension of 10mm (inner radius of 15mm and outer radius of 25mm) and an azimuthal span of 45 degrees. A piezoceramic sensor with a diameter of 5 mm and a thickness of 0·2mm was bonded at the centre of the CLoVER array to record the induced strains. The sensor was bonded by applying a thin layer of Epotek 730 bonding agent. The transducer was excited using a 3·5 Hann-modulated toneburst signal at 65kHz and various peak-to-peak amplitudes. The excitation signal was created using an Agilent 33220A arbitrary waveform generator and amplified using a Krohn-Hite Model 7500 wide band amplifier, while the sensor data were recorded using a digital oscilloscope (Agilent Infinuum 54831DSO).

5.1 Simulated damage I: concentrated mass

The first damage type considered was a concentrated mass located at different radial and azimuthal positions on the surface of the plate. The mass was provided by a metallic bar as shown in Fig. 14. This bar had a square cross section with a side length of 2cm, a height of 25·4cm, and a mass of 1·1kg. In this case, the excitation peak-to peak amplitude was 175V.

At the excitation frequency used in these studies the A_0 mode is dominant. This is advantageous for several reasons. First, the S_0 mode is very weak at low frequencies, which improves the purity of the propagating pulse. Furthermore, the reflections from the simulated damage will also be composed primarily of A_0 components facilitating its identification in the difference signal. Secondly, the dominant out-of-plane component characteristic of the A_0 mode is expected to be more sensitive to the simulated damage being used. Typically, in pulse-echo mode, a baseline sensor response signal corresponding to the pristine condition of the structure is measured using a sensor collocated with the actuator. Subsequently, damage is introduced and the reflections from it exposed by subtracting the baseline result from the signal corresponding to the damaged condition. In this study, the main goal is to evaluate how the reflection amplitude varies with position, and consequently the
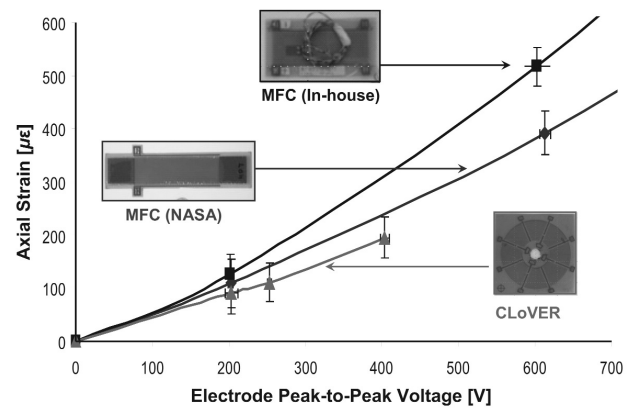

Figure 13. Strain performance comparison among different piezocomposite transducers.
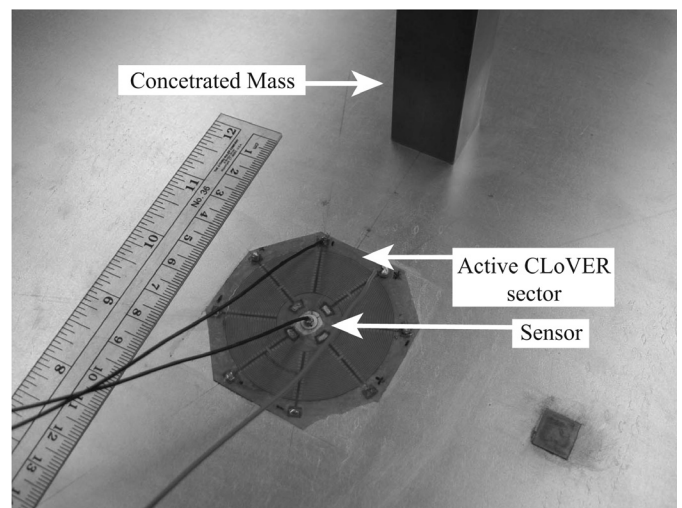

Figure 14. Detail of experimental setup used in damage detection experiments using a concentrated mass.

damage location is assumed to be known *a priori*. Therefore, the group velocity for the A_0 mode, c_g (2324m/s for the specimen used), can be used to estimate the time at which the damage reflection should arrive at the sensor. Since the metallic bar that simulates damage has a significant cross-sectional size, two bounds were calculated for the arrival time. The lower bound assumes that the waves will start reflecting back immediately upon hitting the front of the bar while the upper bound assumes that the reflections will begin once the incoming pulse reaches the back of the bar. The expressions for these times are given by:

$$t_L = \frac{2d_b + d_s}{c_g} + \frac{\overline{T_p}}{2} \qquad \text{...(25)}$$

$$t_U = \frac{2(d_b + L_b) + d_s}{c_g} + \frac{\overline{T_p}}{2} \qquad \text{...(26)}$$

where d_b represents the distance between the damage location (front of the bar) and the outer radial edge of the transducer, d_s represents the distance from the radial edge of the transducer to the sensor, L_b represents the size of the damage, and $\overline{T_p}$ represents the excitation pulse period (used to track the centre of the pulse).

The first set of tests consists of evaluating the decay in reflection amplitude with radial distance in order to gain insight into the inspection distance that can be obtained. In addition, these results are used to select suitable radial positions for the subsequent azimuthal tests that simulate the proposed interrogation approach. The simulated damage was placed at 21 different radial positions, starting at a radial position of $1 \cdot 6R_O$ from the outer radial edge of the transducer in increments of $0 \cdot 4R_O$. A schematic of this setup is shown in Fig. 15(a). Four different data sets were collected at each point, and each of these consisted of 64 averages. Figure 15(b) shows a comparison between the sensor response signal for the pristine and damaged conditions. The excitation pulse and boundary reflections are clearly visible, which allows the time range where

damage reflections are expected to be identified. Sample time histories for the difference signal can be seen in Fig. 16. From these, it is evident that the damage reflection is easily discerned. Furthermore, the time of arrival calculated using the group velocity is in good agreement with the experimental result.

Figure 17 shows how the peak-to-peak amplitude of the damage reflection changes with radial distance. In this case, the error bars correspond to the standard deviation, and the noise level has been indicated by the dashed horizontal line (this corresponds to a response of 2mV peak to peak). Note that for the combination of parameters considered (substrate material and frequency-thickness product), an inspection range in the order of ten times the transducer outer radius can be attained. This in turn corresponds to approximately ten wavelengths for the A_0 mode at the frequency-thickness product tested. It is likely that this distance can be increased for more realistic damage types, where the S_0 mode is used, and by using advanced signal processing algorithms on the inspection signals (see for example Reference (29)). As previously discussed, the A_0 mode has a dominant out-of-plane displacement component which makes it more susceptible to attenuation from structural features or environmental conditions (as for instance fluid loading). In the case considered here, it is likely that part of the energy in the incoming pulse leaks into the bar that provides the simulated damage, thereby reducing the inspection distance that can be attained. It is interesting to note that the reflection amplitude does not decrease monotonically with distance, as would be expected. A similar phenomenon was observed by Diligent *et al*[30] for the case of reflections from part-depth circular defects in plates using the S_0 mode. In that work, it was argued that these oscillations were due to interference between the main reflection from the damage and what they termed secondary reflections, such as circumferential creeping waves and SH_0 waves[30, 31]. From this result, two radial positions were selected for the azimuthal tests which are described next.

The second set of tests simulated the damage interrogation approach presented earlier using CLoVER transducers. In this case however, the damage was manually placed at different azimuthal positions, so as to eliminate any effect associated with possible variations in piezoelectric properties or bond line conditions among
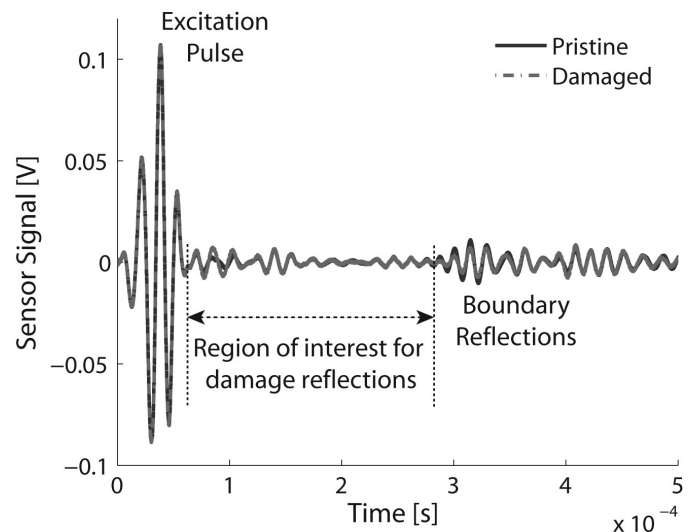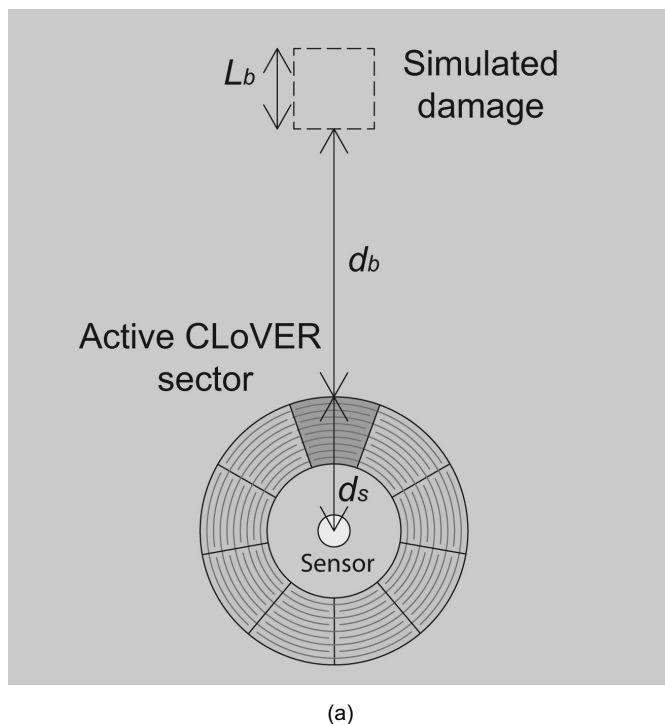

(a)

(b)

Figure 15. (a) Schematic showing damage location for reflection amplitude decay study; (b) Comparison between pristine and damaged sensor response signals for damage located at a radial position of $2R_O$ along the transducer centreline.
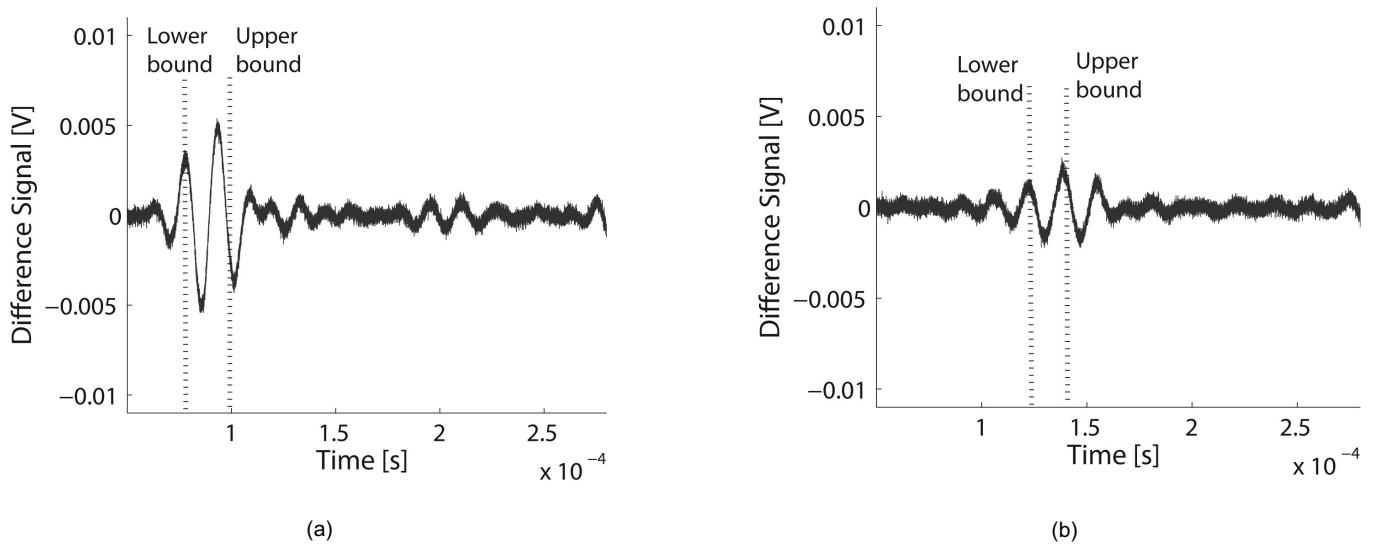
Figure 16. Difference between pristine and damaged sensor response signals for damage located at (a) $2R_O$, and (b) $4R_O$ from the outer radial edge of the transducer.

the sectors. This process is equivalent to maintaining the damage location fixed and sequentially using each CLoVER sector to interrogate the structure. This approach is illustrated in the next subsection. The only parameter not simulated is the time delay between the activation of each sector. This, however, will likely be a fixed parameter primarily dependent on the time needed for all reflections (both from damage and other structural features) to be completely attenuated.

In this case, the distance between the simulated damage and the outer radial edge of the transducer was fixed at two different distances D, $2R_O$ and $4R_O$, while the azimuthal position was varied from $-90°$ to $90°$ in increments of approximately $25°$. As in the previous case, the group velocity for the A_0 mode was used to estimate the time when reflections are expected. These results are shown in Fig. 18 where, as in the previous case, the error bars represent the standard deviation, while the noise level is represented by the black dashed line (note that this level was again selected as 2mV peak-to-peak). In this case, the CLoVER sector's centreline coincides with the $0°$ direction. From the figure it is clear that the input energy to the CLoVER sector is primarily used to detect damage within its azimuthal projection. This illustrates the usefulness of the proposed interrogation approach, as the actuation can be directed primarily along the intended scan direction. This trend is further supported by the similarity in the response values observed for azimuthal positions with an amplitude larger than $50°$, as shown in Fig. 18(b).

5.2 Simulated damage II: through-thickness hole

Four CLoVER sectors (labeled CLoVER sector 1 through CLoVER sector 4) were used in additional simulations of the damage interrogation approach proposed with the CLoVER transducer, as shown in Fig. 19. Each of these was excited using a $3·5$ Hann-modulated toneburst with a centre frequency of 65kHz, where the A_0 mode is dominant. The signal was amplified using a Trek PZD2000 amplifier and its peak-to peak amplitude was slightly different for each sector to ensure that the peak-to-peak amplitude of the main pulse received by the sensor was similar for all of them (the variations in the input voltage were within 50V among all the sectors). As in the previous case, the only parameter not simulated in this study is the time delay that exists between alternating sectors, as they were activated manually.
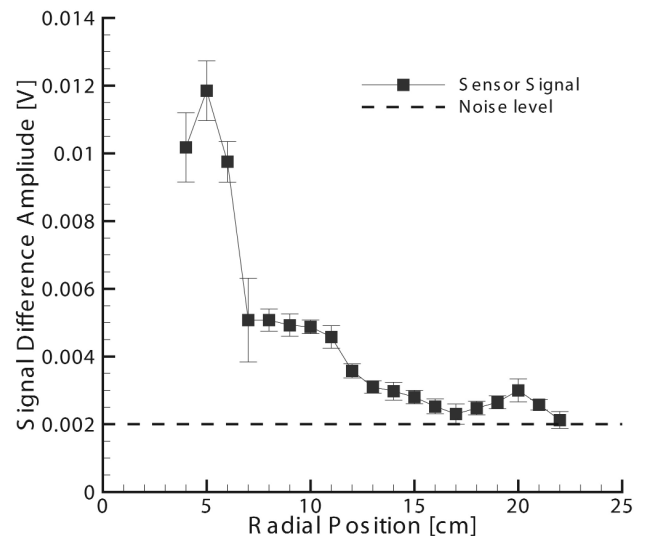

Figure 17. Variation of damage reflection amplitude with radial position along the transducer centreline.

A through-thickness hole with a diameter of $4·8$mm was drilled at a radial distance of $4R_O$ away from the radial edge of one CLoVER sector to simulate structural damage, as also shown in Fig. 19. The same isotropic plate structure and CLoVER transducer used in the previous cases was employed here. The diameter of the hole to wavelength ratio was approximately $0·25$. This dimension was selected so that the reflections from the front and back of the hole would interfere constructively as shown by Diligent[30] for the case of part-depth holes. However, it is expected that the reflection amplitude from a through-hole should increase monotonically with dimension as also discussed by Diligent *et al*[32]. The damage location was again detected using the pulse-echo mode, and the same piezoelectric sensor used in the previous section was employed. By again assuming the location of the damage to be known, the following expression for the time-of-arrival of the damage reflection is obtained:
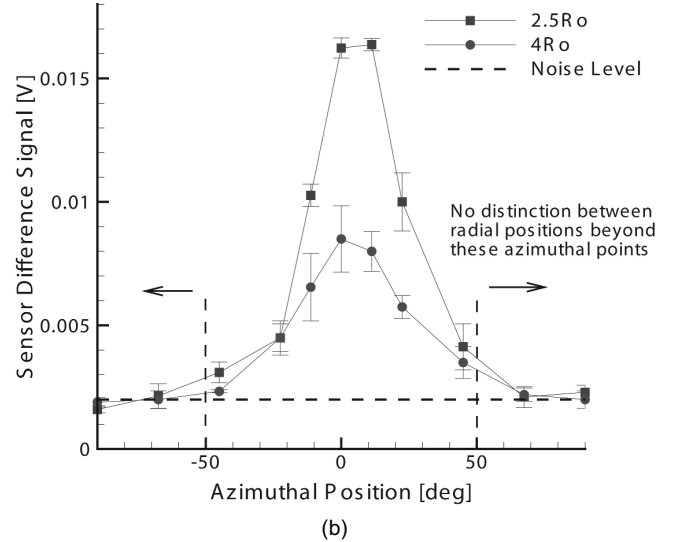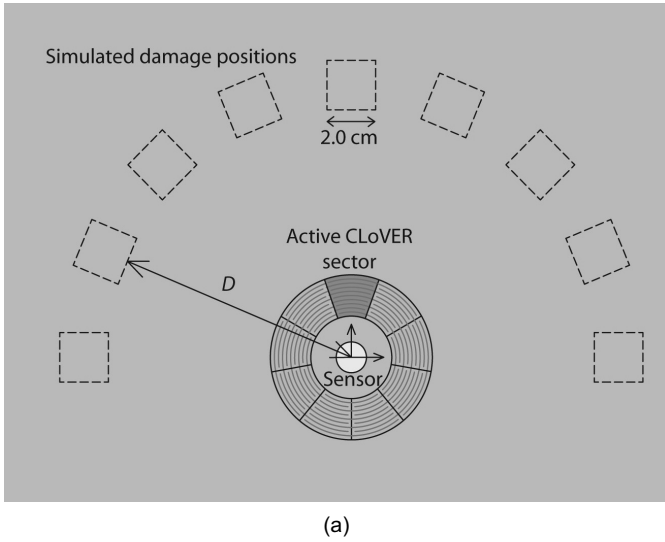
(a)

(b)

Figure 18. (a) Schematic showing simulated damage locations for azimuthal tests;
(b) Variation of damage reflection amplitude with azimuthal position for various radial locations.

$$t_r = \frac{2d_h + R_O}{c_g} + \frac{\overline{T_p}}{2} \qquad \qquad ...(27)$$

In preliminary studies it was found that the times of arrival obtained assuming the reflections originated at the front of the hole were very similar to those obtained assuming they originated at the back. Consequently, only the value corresponding to the front of the hole was used to track the damage reflections. It has been previously reported that the S_0 mode is more sensitive to through-the-thickness damage due to its dominant in-plane components[7], [16]. However, in order to excite a pure symmetric mode two transducers are typically needed (one on each surface of the substrate). When these are excited in phase, the S_0 mode propagates in the plate, while if the A_0 mode is desired, they are excited out of phase. Some of the CLoVER sectors on one of the transducers employed were unavailable for testing as they had sustained damage during earlier electric poling tests, therefore making the excitation of symmetric modes for all sectors impossible. Consequently, the present study uses the A_0 mode to provide a concept demonstration of the proposed damage interrogation approach.

Figure 20(a)-(d) shows sample difference signals collected with the piezoelectric sensor where the expected time of arrival for the A_0 mode defect reflections is highlighted. Two measurements were taken with each sector and 128 averages were collected in each of these. The peak-to-peak value in the region where the reflection is expected was measured, and the result is summarised in Fig. 21. The results presented correspond to average values, while the error bars represent three times the standard deviation. Each of these signals was post-processed by removing linear and constant trends and passed through a bandpass filter. The maximum amplitude is recorded when CLoVER sector 2 is activated, which is the expected result as the damage is located along this sector's centreline. Furthermore, the reflection amplitude for the remaining sectors decreases with increasing index (for sectors 3 and 4), as the centreline of these transducers moves farther away from the damage location. Note in particular that the signal recorded when CLoVER sector 4 was used does not appear to have a significant contribution at the expected arrival time. This observation is expected as the wave field induced by this sector is very small near the damage location. This result illustrates the improvement offered by the interrogation approach attainable with the CLoVER transducer, as with prior knowledge of the device's configuration (namely the azimuthal
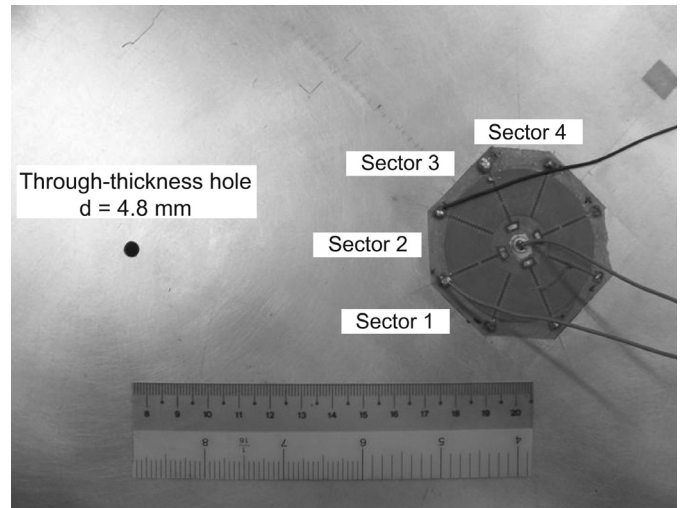

Figure 19. Detail of through-thickness hole introduced for damage interrogation approach demonstration.

direction of each sector), information about the presence of damage can be inferred. Note that in this particular experimental test, only four transducers were required to interrogate a structural area spanning 180° degrees. Furthermore, due to the directionality of the transducer and the geometry of the device, the azimuthal location of the defect relative to the CLoVER transducer can be easily identified without phased addition or other post-processing algorithms.

5.3 Laser vibrometer tests

The interaction between the GW field excited by the CLoVER transducer and the through-thickness hole was examined in more detail using laser vibrometry. This non-contact technique is able to provide information near the location of the defect. The objective is to show that the GW interaction with the simulated damage stays predominantly within the azimuthal projection of the CLoVER sector whose centreline is best aligned with the damage site. The key instrument used was a Polytec PSV-400 scanning laser vibrometer, which is composed of the PSV-I-400 scanning head, the OFV-5000 controller, the PSV-E-401 junction box, and a data management system. The light source used in the PSV-400 is a helium neon laser that provides a linear polarised beam[33]. The vibrometer system is
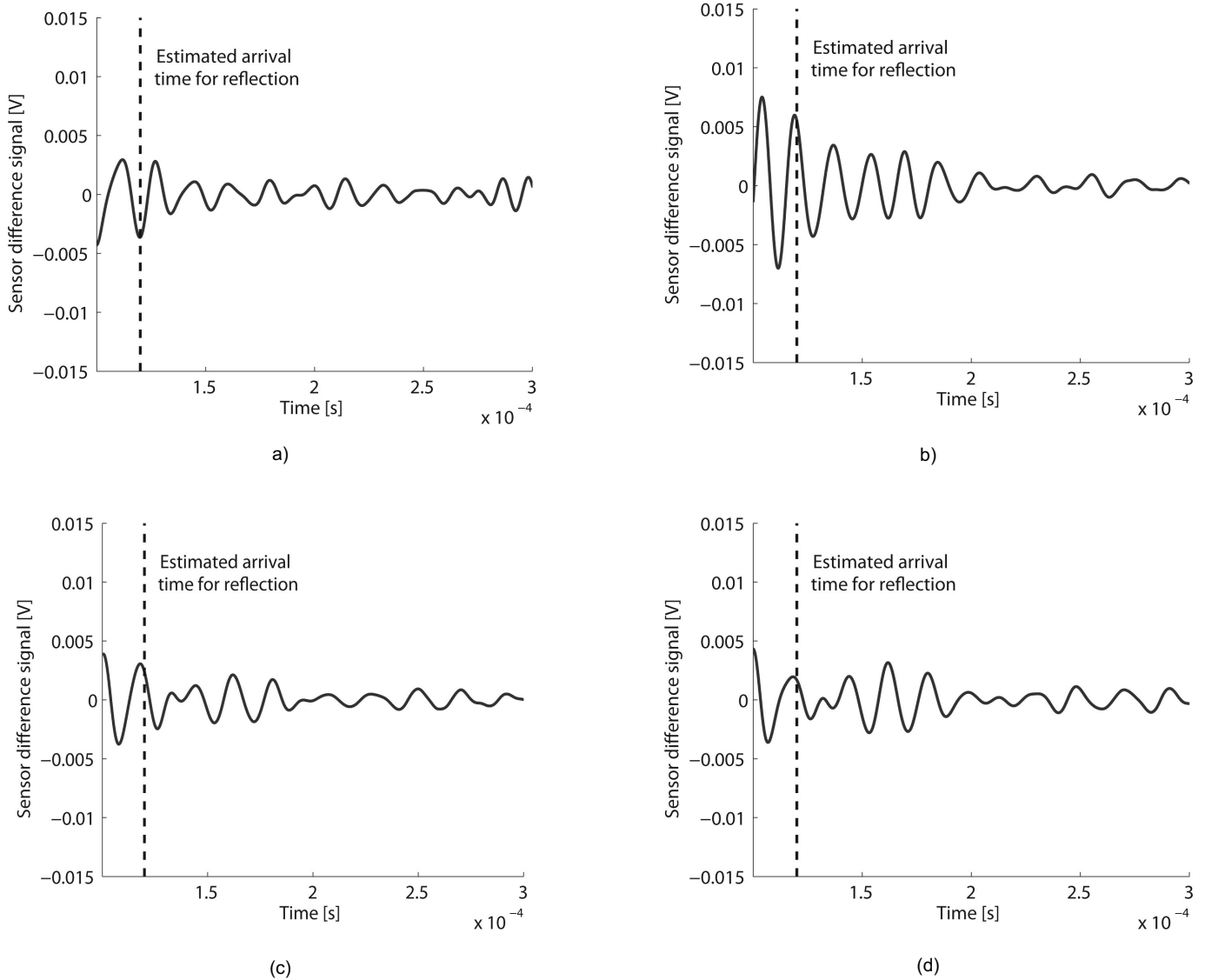
Figure 20. Difference signal between pristine and damaged conditions for
(a) CLoVER sector 1 (b) CLoVER sector 2 (c) CLoVER sector 3 (d) CLoVER sector 4.

able to measure the out-of-plane velocities by measuring the difference in path lengths between a reference beam and an object beam that is backscattered from the surface under inspection. The scanning head was supported using a tripod and maintained at a distance of 915mm from the scanning surface for most of the experimental tests conducted. This distance was selected to operate at a laser visibility maximum[33]. The overall experimental setup used in these tests is shown in Fig. 22(a) while a block diagram illustrating the interaction among the different components is shown in Fig. 22(b). The process begins by generating an excitation pulse which is amplified through a Trek PZD2000 amplifier. At the same time, the PSV system is triggered and laser parameters from the PSV-I-400 scanning head start being recorded. The phase difference produced in the incident laser beam by the surface motion is relayed to the controller, via the junction box, where it is decoded into a velocity signal. This result is later relayed through the junction box to the data management system where it is visualised via the PSV software. The sampling frequency used in this case was 5·12MHz.

In the case of laser vibrometry, pulse-echo type of approaches where a signal corresponding to the pristine condition is compared to one after damage has been introduced cannot be easily implemented. This would require positioning the laser at exactly the same location
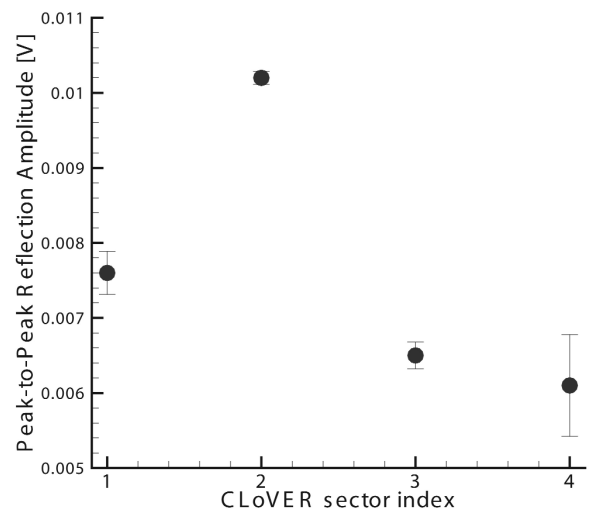

Figure 21. Comparison of reflection amplitudes
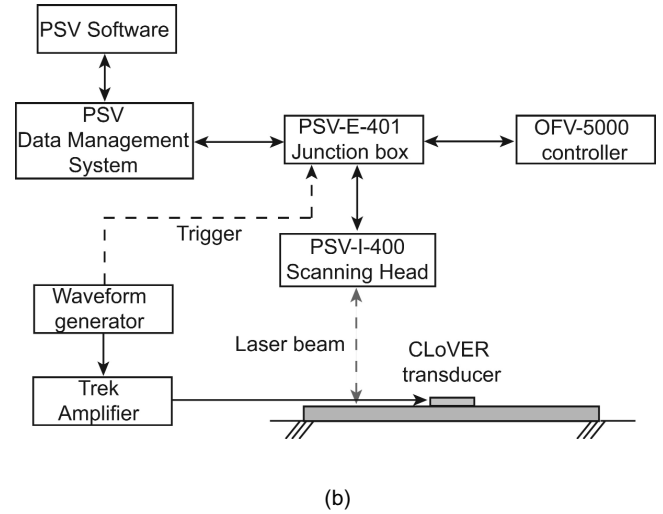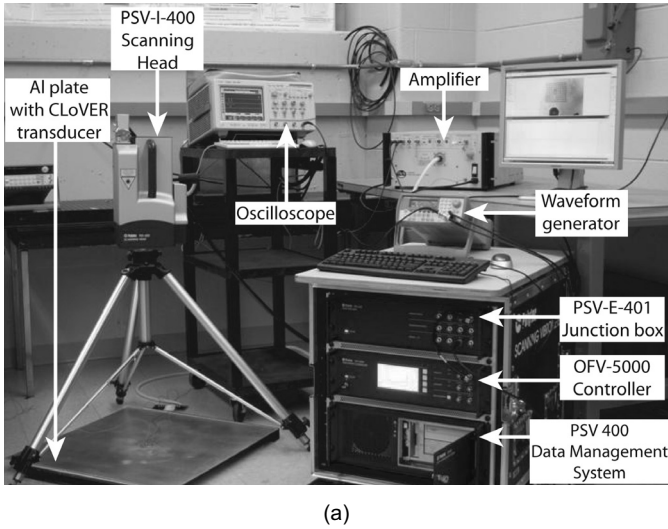among different CLoVER sectors.

Figure 22. (a) Overall arrangement for laser vibrometer experiments;
(b) Block diagram illustrating the interaction among the different setup components.
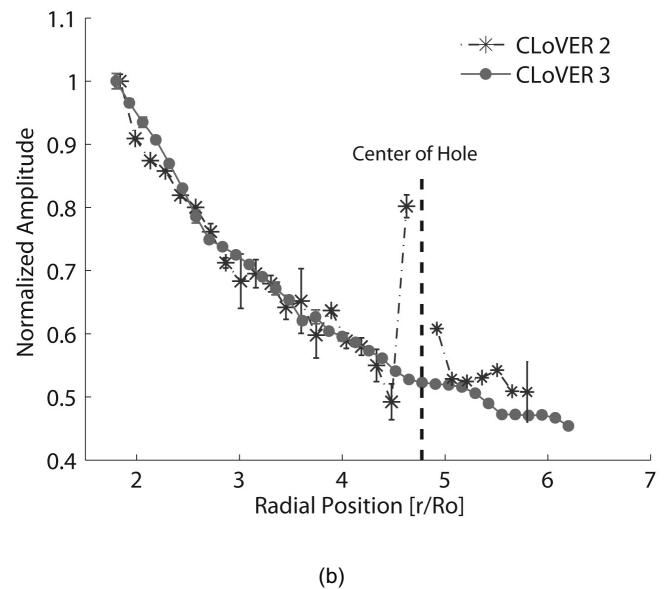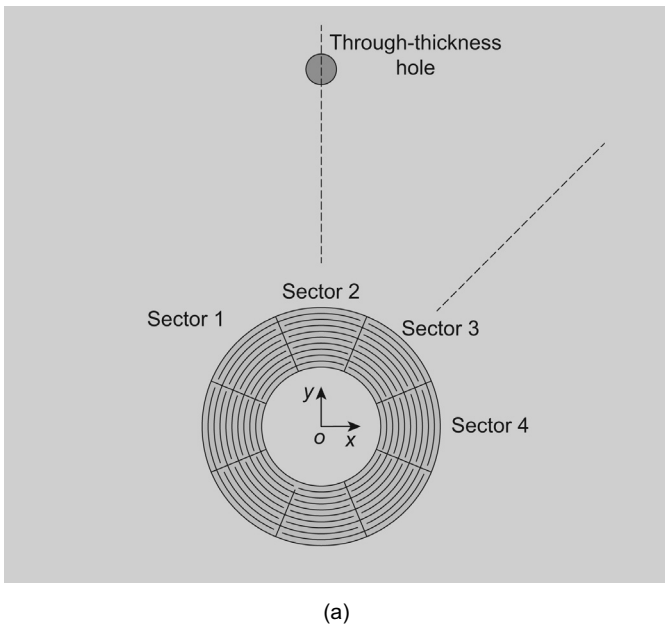

Figure 23: (a) Schematic illustrating the location of the laser measurement points in the amplitude attenuation studies;
(b) Effect of through-thickness hole on incident GW field for CLoVER sectors 2 and 3.

on the surface of the inspected structure before and after the damage has been introduced. Since the laser beam diameter is very small (~ 130µm for the middle range lens at the separation distance between the laser and specimen used[33]), this is nearly impossible to achieve as small positioning errors inevitably result during the introduction of damage. Consequently, the first set of tests consisted of evaluating the decay in peak-to-peak amplitude of the propagating pulse along the centreline of different CLoVER sectors. This test provides insight into how the presence of the hole influences the propagating pulse. Two different CLoVER sectors were considered, as shown in Fig. 23(a), with the first of them aligned with the damage and the second one located adjacent to the first one. The result is shown in Fig. 23(b), where the effect of the hole on the incoming pulse is clearly visible. In this case only a relative comparison is sufficient, and the results have been normalised by the maximum value in each data set. The data points represent average values while the error bars represent three times the standard deviation, which was calcu-

lated based on two separate measurements with 64 averages each. The result shows that the hole produces an increase in amplitude only very close to its edge when the transducer aligned with it is used. The result observed for the case of CLoVER sector 2 is consistent with the results reported by Mallet et al[34] for the interaction of axisymmetric GW fields with rectangular notches and circular defects in aluminum plates using laser vibrometry.

The second set of tests consisted of measuring the peak-to-peak amplitude for points located on a circle whose radius coincides with the position of the hole, as shown in Fig. 24(a). The same CLoVER sectors as in the previous case were used, and the results are shown in Fig. 24(b). In this case, the raw data are presented as the maximum value in the data set collected is expected to occur where the damage is located, and therefore a baseline value is not available. Note that the effect of the hole is predominant within azimuthal projection of CLoVER sector 2, whose centreline is aligned with the damage site. It can also be observed that the hole appears to have a
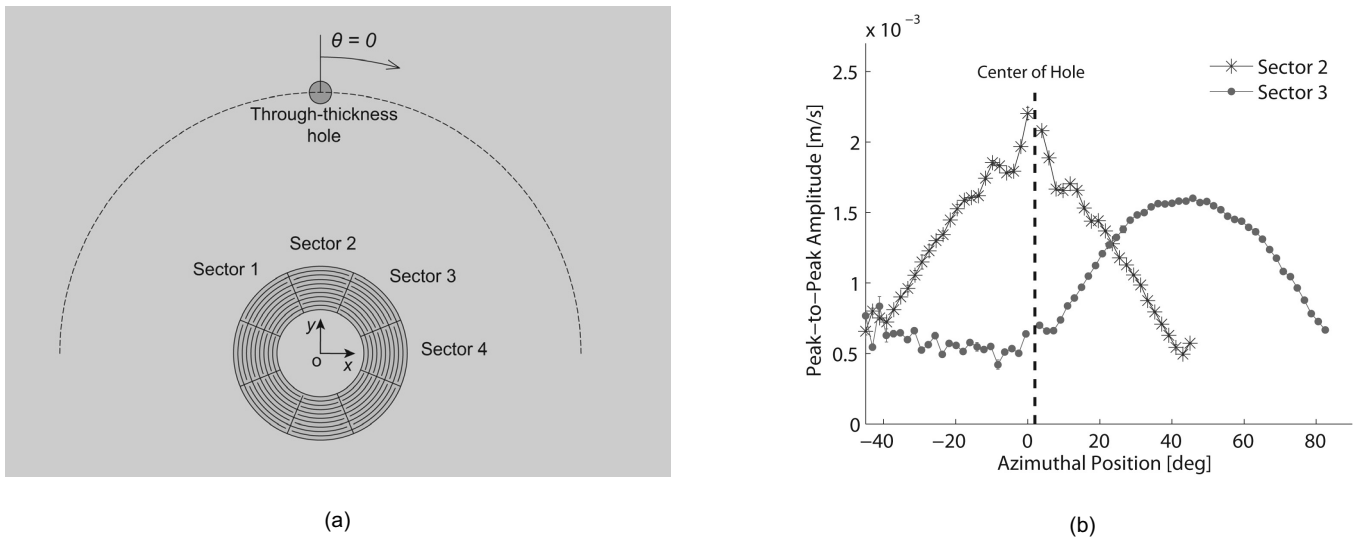
(a)

(b)

Figure 24: (a) Schematic illustrating the location of the laser measurement points in the azimuthal tests; (b) Effect of through-thickness hole on azimuthal distribution of incident GW field for CLoVER sectors 2 and 3.

weak effect on the GW field induced by CLoVER sector 3, but this occurs in a region of small wave amplitudes where the uncertainty in the measurements is larger. A two-dimensional presentation of these results is given in Fig. 25 where the peak-to-peak amplitude of the out-of-plane velocities is shown in the region surrounding the through-thickness hole. The main conclusion from the previous tests is that the presence of the defect is most clearly visible when the sector whose centreline is best aligned with its position is employed. This characteristic demonstrates that the input energy to a CLoVER sector is efficiently used, and will play a key role in the design of damage detection algorithms using these transducers.

6.0 CONCLUSIONS

The Composite Long-range Variable-direction Emitting Radar (CLoVER) transducer was introduced in this paper as an alternative concept for guided wave (GW) based structural health monitoring (SHM) systems. This novel device is composed of individual wedge-shaped anisotropic piezocomposite sectors operating under the 3-3 piezoelectric effect, therefore producing directional GW fields. The theory of GW excitation by a CLoVER sector was reviewed and used in multiple parametric studies related to the dimensions of the transducer. The in-house fabrication procedure for CLoVER transducers was described, and the devices were used in multiple damage detection experiments in isotropic plate structures. The following conclusions can be drawn from this study:

● Experimental results in isotropic plates demonstrated that the geometric arrangement of the CLoVER transducer combined with the directionality of each segment provide an improved damage interrogation methodology for GW SHM systems. This approach is capable of detecting and locating structural defects (simulated through a concentrated mass and through-thickness hole) over a complete structural surface (360° range) from a central location with a reduced number of transducers and efficient use of the input energy.

● The geometry of a CLoVER sector allows the electric input to the device to be more efficiently used than in conventional configurations. It was shown that the actuation amplitude can be increased relative to a ring configuration by a factor given by the ratio of the azimuthal span of a CLoVER sector and a ring for similar electric current inputs. Specific examples for the
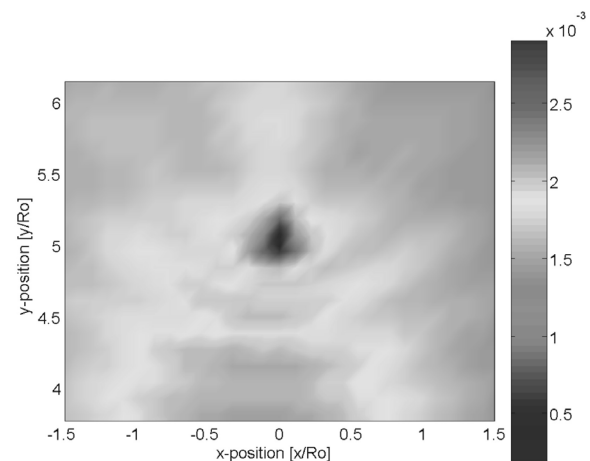

Figure 25. Interaction of incident GW field with structural defect: peak-to-peak amplitude of out-of-plane velocity component near the through-thickness-hole.

fundamental symmetric and antisymmetric modes indicated that the displacements could be increased by as much as a factor of eight for the frequency-thickness products considered.

● The radial dimension of the CLoVER transducer dominates its performance in the frequency domain. In particular, the response exhibits local minima when the radial dimension coincides with integer multiples of the mode wavelength, while local maxima occur for dimensions of 0·35-0·5 integer multiples of the wavelength.

● The transducer inner to outer radius ratio is critical to its response in the frequency domain. This parameter should be selected in the order of 0·9 to attain modal selectivity, and in the order of 0·2 to obtain a transducer with large gain over a wide frequency range.

● The azimuthal dimension of the transducer has a secondary effect on its frequency response for values lower than 90°.

● The in-house fabrication procedure for CLoVER transducers presented in this work is effective in producing devices with free-strain performance characteristics similar to those in conventional piezocomposite devices.

ACKNOWLEDGEMENTS

REFERENCES

1. RAGHAVAN, A. and CESNIK, C.E.S. Review of guided-wave based structural health monitoring, *The Shock and Vibration and Digest*, March 2007, **39**, (2), pp 91-114.
2. BENT, A.A. and HAGOOD, N.W. Anisotropic actuation with piezoelectric fibre composites, *J Intelligent Materials Systems and Structures,* May 1995, **6**, (3), pp 338-349.
3. BENT, A.A. Active Fibre Composites for Structural Actuation, Ph.D. thesis, Massachusetts Institute of Technology, Cambridge, MA, 1997.
4. WILKIE, W.K. and HIGH, J.W. Method of fabricating NASA-standard macro-fibre composite piezoelectric actuators, National Aeronautics and Space Administration, Technical Report NASA/TM-2003-212427, 2003.
5. WILCOX, P.D., CAWLEY, P. and LOWE, M.J.S. Acoustic fields from PVDF interdigital transducers, *IEEE Proceedings on Science Measurement Technology,* September 1998, **45**, (5), pp 250-259.
6. WILCOX, P.D., LOWE, M.J.S. and CAWLEY, P. Omnidirectional guided wave inspection of large metallic plate structures using an EMAT array, *IEEE Transactions on Ultrasonics Ferroelectrics and Frequency Control,* April 2005, **52**, (4), pp 653-665.
7. WILCOX, P.D., LOWE, M.J.S. and CAWLEY, P. Lamb and SH transducer arrays for the inspection of large areas of thick plates, Review of Progress in Quantitative Nondestructive Evaluation Conference Proceedings, May 2000, Paper #509A.
8. FROMME, P., WILCOX, P.D., LOWE, M.J.S. and CAWLEY, P. On the development and testing of a guided ultrasonic wave array for structural health monitoring, *IEEE Transactions on Ultrasonics Ferroelectrics and Frequency Control,* April 2006, **53**, (4), pp 777-785.
9. YU, L. and GIURGIUTIU, V. Design, implementation, and comparison of guided wave phased arrays using embedded piezoelectric wafer active sensors for structural health monitoring, Proceedings of the 13th SPIE Symposium on Smart Structures and Materials & Nondestructive Testing and Health Monitoring, March 2006, San Diego, CA.
10. YU, L., GIURGIUTIU, V. and KENDALL, J.R. Omnidirectional guided wave PWAS phased array for thin-wall structure damage detection, Proceedings of the 14th SPIE Symposium on Smart Structures and Materials & Nondestructive Testing and Health Monitoring, March 2007, San Diego, CA.
11. KIM, D. and PHILEN, M. On the Beamsteering characteristics of MFC phased arrays for structural health monitoring, Proceedings of the 49th AIAA/ASME/ASCE/AHS/ASC Structures Structural Dynamics and Materials Conference, April 2008, Paper # AIAA-2008-1969, Schaumburg, IL.
12. ZEMMOUR, A.I. The Hilbert-Huang Transform for Damage Detection in Plate Structures, MS thesis, University of Maryland, College Park, MD, 2006.
13. MATT, H.M. and LANZA DI SCALEA, F. Macro-fibre composite piezoelectric rosettes for acoustic source location in complex structures, *Smart Materials and Structures,* August 2007, **16**, (4), pp 1489-1499.
14. CESNIK, C.E.S. Integrated Vehicle Health Management NASA Task 5C Annual Report, Proceedings of the NASA Reusable Launch Vehicle URETI, April 2003, Cleveland, OH.
15. SALAS, K.I. and CESNIK, C.E.S. Design and Characterization of the CLoVER transducer for structural health monitoring, Proceedings of the 15th SPIE Symposium on Smart Structures and Materials & Nondestructive Testing and Health Monitoring, March 2008, Paper #6935-11, San Diego, CA.
16. ALLEYNE, D. and CAWLEY, P. The interaction of Lamb waves with defects, *IEEE Transactions on Ultrasonics Ferroelectrics and Frequency Control,* May 1992, **39**, (3), pp 381-397.
17. SALAS, K.I., CESNIK, C.E.S. and RAGHAVAN, A. Modeling of wedge-shaped anisotropic piezocomposite transducer for guided wave-based structural health monitoring, Proceedings of the 15th AIAA/ASME/AHS Adaptive Structures Conference, April 2007, AIAA Paper # AIAA-2007-1999, Honolulu, HI.
18. SALAS, K.I. and CESNIK, C.E.S. Guided wave excitation by a CLoVER transducer for structural health monitoring: theory and experiments, *Smart Materials and Structures* (in press).
19. CRAWLEY, E.F. and DE LUIS, J. Use of piezoelectric actuators as elements of intelligent structures, *AIAA J*, October 1987, **25**, (10), pp 1373-1385.
20. CHAUDRY, P. and ROGERS, C.A. The Pin-Force model revisited, *J Intelligent Materials Systems and Structures,* May 1994, **5**, (3), pp 347-354.
21. NGUYEN, C.H. and KORNMANN, X. A comparison of dynamic piezoactuation of fibre-based actuators and conventional PZT patches, *J of Intelligent Materials Systems and Structures,* January 2006, **17**, (1), pp 45-55.
22. LLOYD, J.M. Electrical properties of macro-fibre composite actuators and sensors, M.S. thesis, Virginia Polytechnic Institute and State University, Blacksburg, VA, 2004.
23. Loctite Research, Development, and Engineering, *Technical Data Sheet for Hysol 9491,* http://www.loctite.com, 2003.
24. Engineering Fundamentals Material Database. http://www.efunda.com/materials/piezo, 2007.
25. WILKIE, W.K., BRYANT, R.G., HIGH, J.W., FOX, R.L., HELLBAUM, R.F., JALINK, A., LITTLE, B.D. and MIRICK, P.H. Low-cost piezocomposite actuator for structural control applications, *Proceedings of the SPIE,* March 2000, **3991**.
26. WILKIE, W.K., INMAN, D.J., LLOYD, J.M. and HIGH, J.W. Anisotropic laminar piezocomposite actuator incorporating machined PMN-PT single-crystal fibres, *J Intelligent Materials Systems and Structures,* January 2006, **17**, (1), pp 15-28.
27. WILLIAMS, R.B., GRIMSLEY, B.W., INMAN, D.J. and WILKIE, W.K. "Manufacturing and cure kinetics modeling for macro-fibre composite actuators, *J Reinforced Plastics and Composites,* November 2004, **23**, (16), pp 1741-1754.
28. WILLIAMS, R.B. Nonlinear Mechanical and Actuation Characterization of Piezoceramic Fibre Composites, Ph.D. thesis, Virginia Polytechnic Institute and State University, Blacksburg, VA, 2004.
29. RAGHAVAN A. and CESNIK, C.E.S. Guided wave signal processing using chirplet matching pursuits and mode correlation for structural health monitoring, *Smart Materials and Structures*, April 2007, **16**, (2), pp 355-366.
30. DILIGENT, O. and LOWE, M.J.S. Reflection of the S_0 Lamb mode from a flat bottom circular hole, *J Acoustical Society of America*, November 2005, **118**, (5), pp 2869-2879.
31. DILIGENT, O. Interaction Between Fundamental Lamb Modes and Defects in Plates, PhD thesis, Imperial College of Science Technology and Medicine, London, UK, 2003.
32. DILIGENT, O., GRAHN, T., BOSTROM, A., CAWLEY, P. and LOWE, M.J.S. The low-frequency reflection and scattering of the S_0 Lamb mode from a circular through-thickness hole in a plate: finite element analytical and experimental studies, *J Acoustical Society of America*, December 2002, **112**, (6), pp 2589-2601.
33. Polytec GmbH. *Polytec Scanning Laser Vibrometer PSV 400 Hardware Manual,* 2007
34. MALLET, A., LEE, B.C., STASZEWSKI, W.J. and SCARPA, F. Structural health monitoring using scanning laser vibrometry: II. Lamb waves for damage detection, *Smart Materials and Structures*, April 2004, **13**, (2), pp 261-269.